

Neurobiophysics

lec 1

2017



Izhikevich, 2007

What the course is about

- **Goal:** to learn about theoretical and computational neuroscience. Build a model of thousands of neurons with synaptic connections
- Focus/scope:
 - Theoretical (bio): physiology of neurons, astrocytes, and synaptic connections
 - Theoretical (math): bifurcations and excitability
 - Numerical: Conductance-based and simplified models of neurons, models of synapses

Is there a difference between neuro-biophysics and theoretical neuroscience / comp.neurosci?

- *Biophysics* — is a science about mechanisms, about processes and their interactions, their role in biological phenomena
- Thus, the course:
 - Rooted in biophysical understanding of physiology and electrical properties
 - Not exclusively computational neuroscience (but based on)
 - Not dynamical systems course (but we'll need that)

Scales

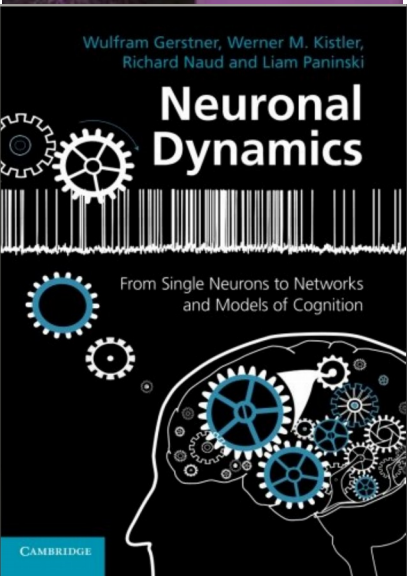
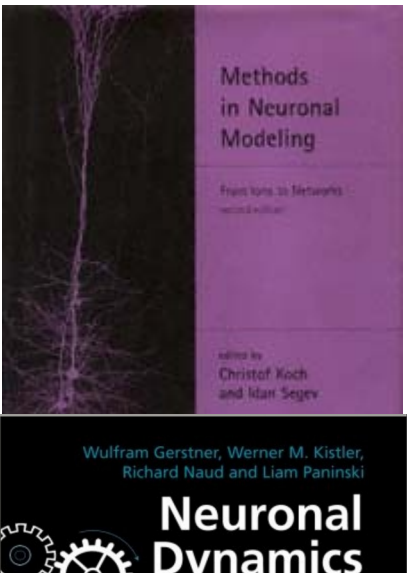
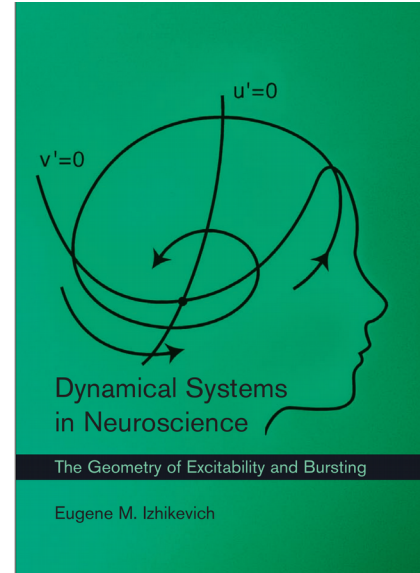
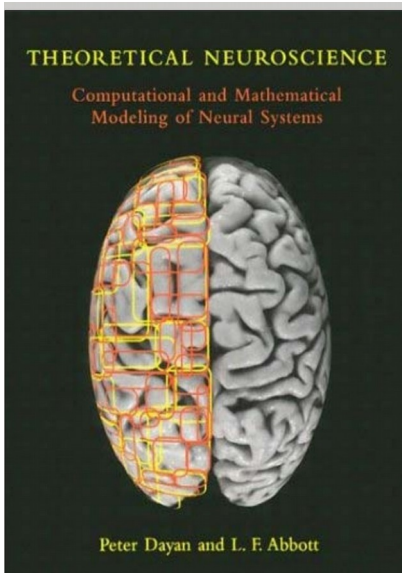
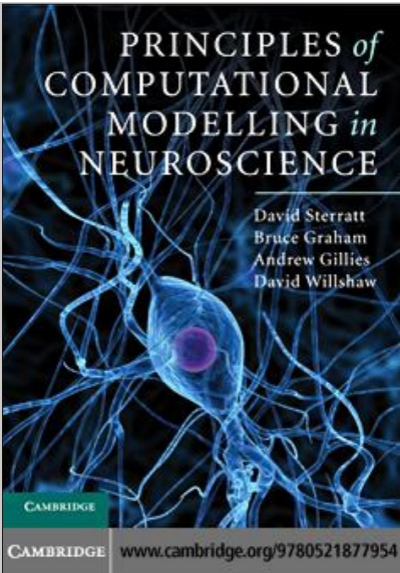
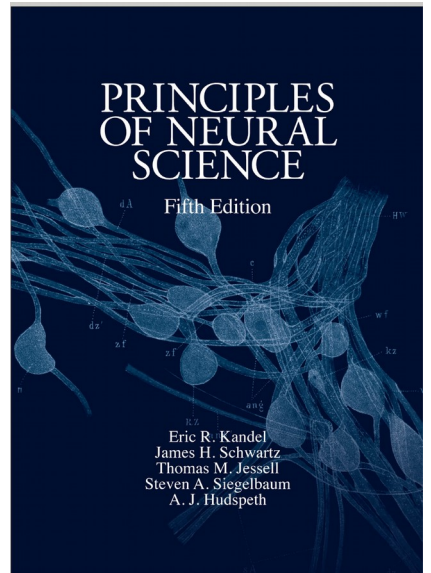
- Single molecules (channels, receptors) — their kinetics and molecular structure → dynamics of molecular ensembles →
- Subcellular structures: synapses, dendritic spines, etc →
- Ion currents/flows from subcellular compartments to whole cells →
- Electrical activity of individual cells and cell-to-cell connections →
- Network activity

At each level some assumptions and simplifications are required

Outline

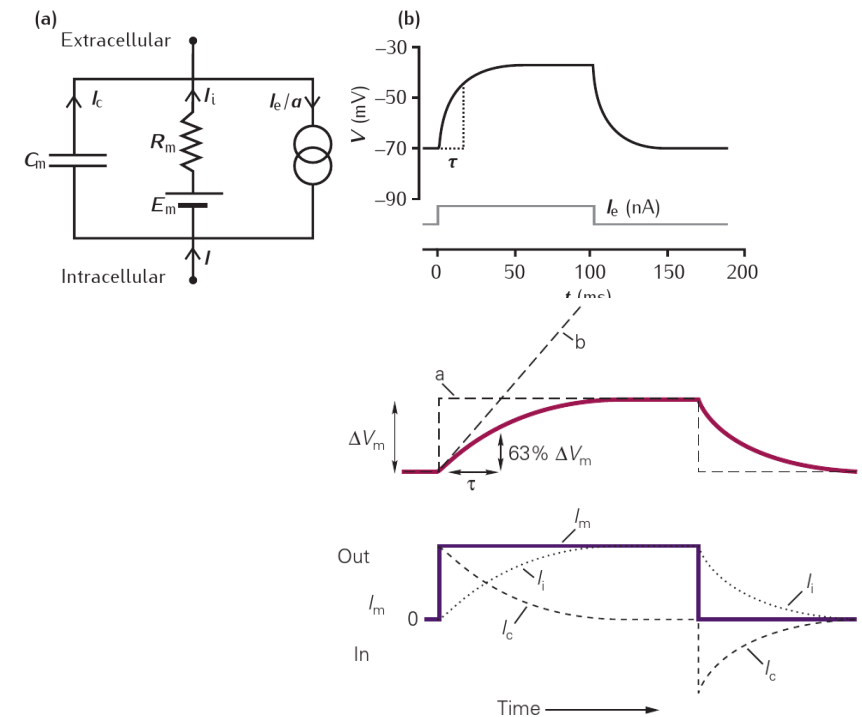
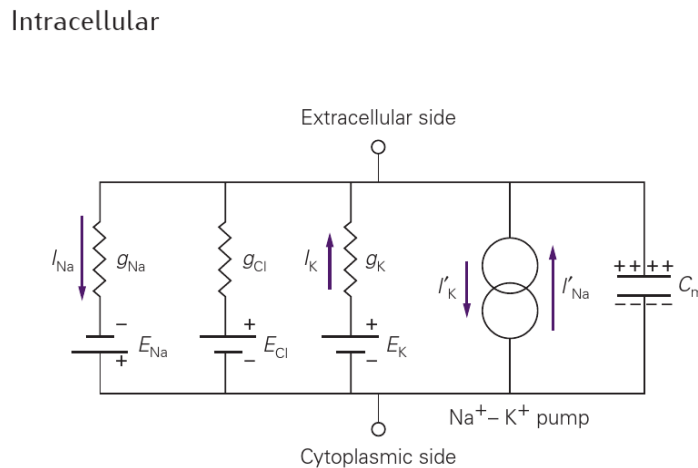
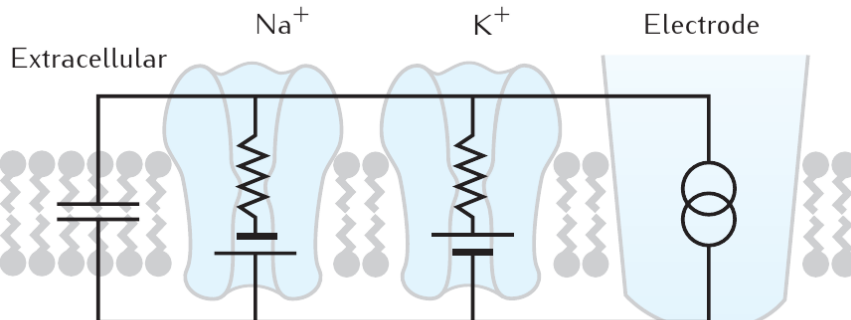
- 7 theoretical lectures and 7-8 modeling modules
- The Hodgkin-Huxley formalism and conductance-based models, simplified models and phase-plane analysis
- Physiology and biophysics of synaptic transmission
- Models of synaptic transmission: vesicle release, receptor kinetics and plasticity
- Information flow & Energy supply **OR** analysis of experimental (imaging) data

Some recommended literature



Overview and trailers (spoilers!!!)

Passive electrical properties of membranes



Measuring electrical properties of a membrane

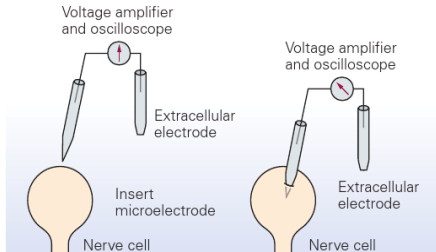


Figure 6-2A The recording setup.

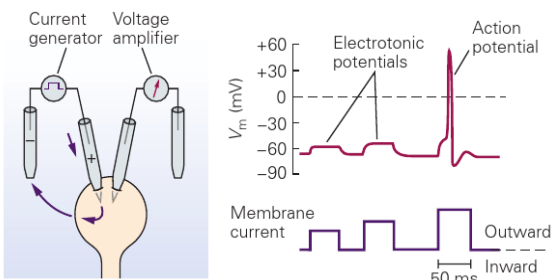


Figure 6-2C Depolarization.

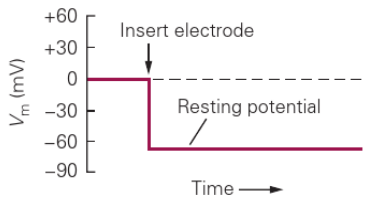


Figure 6-2B Oscilloscope display.

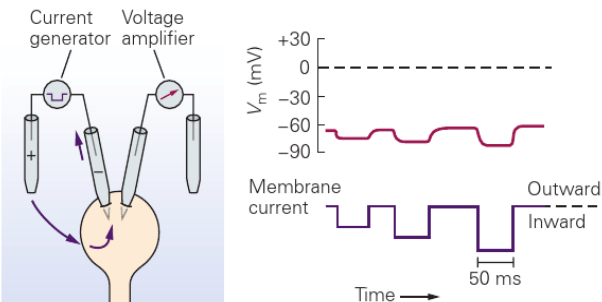
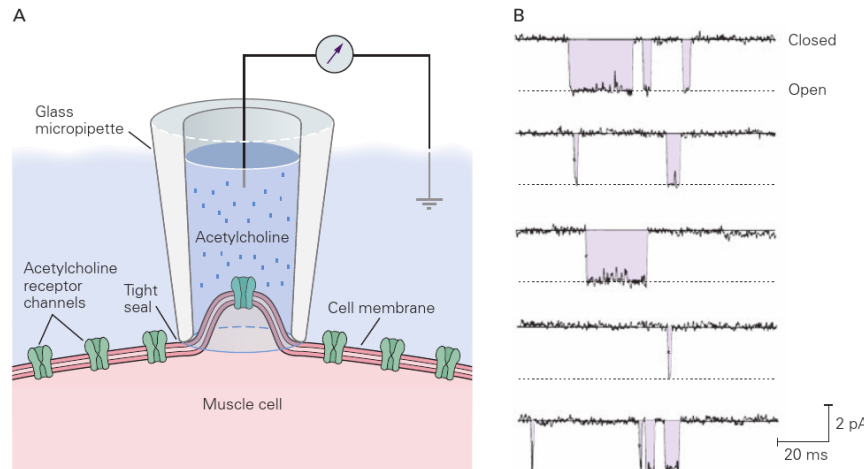


Figure 6-2D Hyperpolarization.



Electrochemical potential and electrodiffusion

Electrochemical potential

$$\bar{\mu} = \mu_0 + RT \ln C + zF\phi$$

C : concentration
 z : ion charge
 F : Faraday's constant
 R : universal gas constant
 ϕ : electrical potential

Flow

concentration	motivating force	motility
---------------	------------------	----------

$$J = C \left(-\frac{d\mu}{dx} \right) u = -Cu \left(RT \frac{1}{C} \frac{dC}{dx} + zF \frac{d\phi}{dx} \right)$$

$$\left[\frac{\text{mole}}{\text{cm}^2 \text{s}} \right] J = -uRT \frac{dC}{dx} - uCzF \frac{d\phi}{dx}$$

Nernst-Planck equation

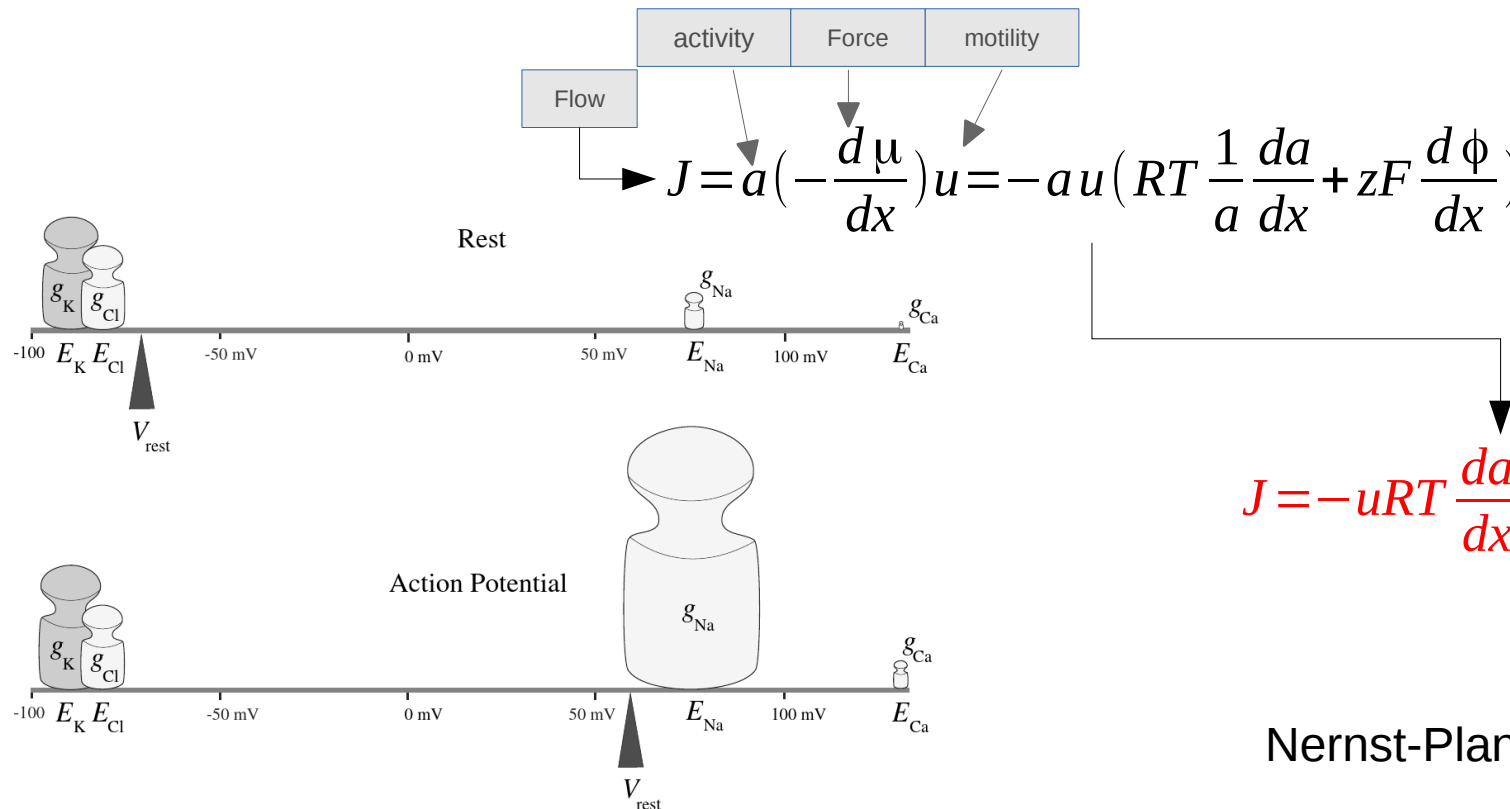
Ficks's law

Electrochemical potential and electrodiffusion

Electrochemical potential

$$\bar{\mu} = \mu_0 + RT \ln a + zF \phi$$

a : activity
 z : ion charge
 F : Faraday's constant
 R : universal gas constant
 ϕ : electrical potential



Nernst-Planck equation

Constant-field approximation (GHK)

$$J = C \left(-\frac{d\mu}{dx} \right) u = -u \left(RT \frac{dC}{dx} + CzF \frac{d\phi}{dx} \right);$$

constant field approximation

$$\frac{d\phi}{dx} = const = \frac{\Delta\phi}{h}$$

C', C'' — ion concentrations on the membrane interfaces

$$C_i = \gamma C' \quad \text{separation coefficient}$$

$$C_o = \gamma C''$$

$$P = uRT \frac{\gamma}{h} \quad \text{permeability}$$

$$\frac{dC}{dx} + C \frac{zF \Delta\phi}{hRT} = \frac{-J}{uRT}$$

$$\frac{dC}{dx} = a + bC$$

$$\int_{C'}^{C''} \frac{dC}{a + bC} = \int_0^h dx$$

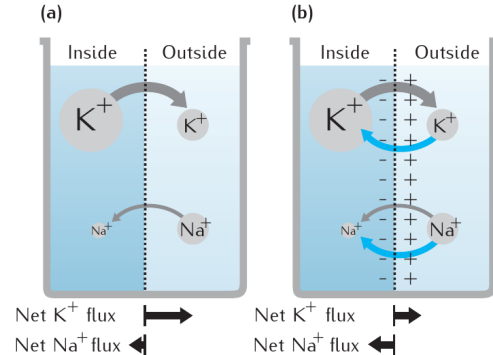
$$\frac{1}{b} \ln \frac{a + bC''}{a + bC'} = h$$

$$J = \frac{zF}{h} \frac{C' - C'' e^{-zF \Delta\phi / RT}}{1 - e^{-zF \Delta\phi / RT}}$$

$$\left[\frac{\text{mole}}{\text{cm}^2 \text{s}} \right] J = P \frac{zF}{RT} \frac{C_i - C_o e^{-zF \Delta\phi / RT}}{1 - e^{-zF \Delta\phi / RT}},$$

$$I = zFJ$$

Goldman-Hodgkin-Katz equation for ion flow



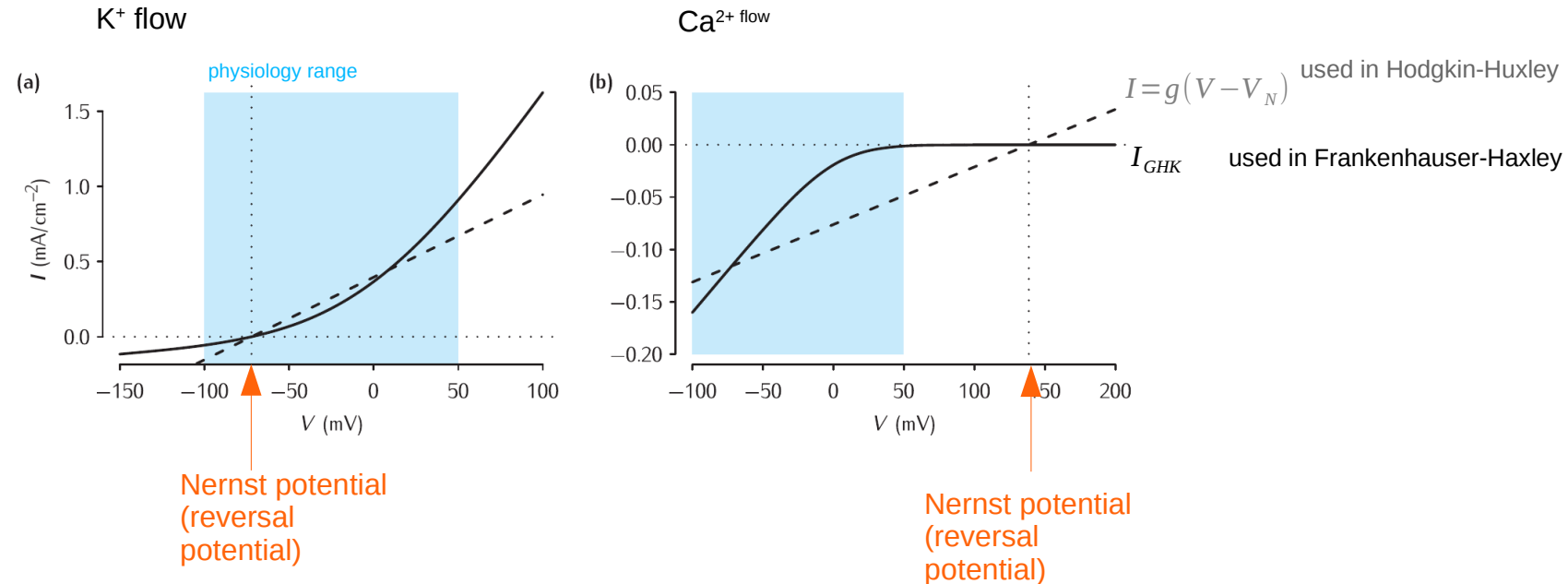
Equilibrium for net current,
not individual currents

Goldman equation for resting potential

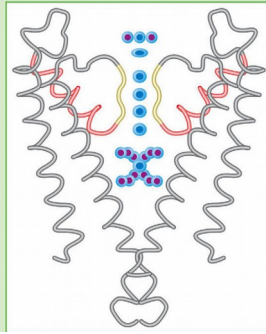
$$\sum_k I_k = 0$$

$$\Delta\phi = \frac{RT}{F} \ln \frac{\sum_k P_k [Cat]_{k\text{out}} + \sum_k P_k [Ani]_{k\text{in}}}{\sum_k P_k [Cat]_{k\text{in}} + \sum_k P_k [Ani]_{k\text{out}}}$$

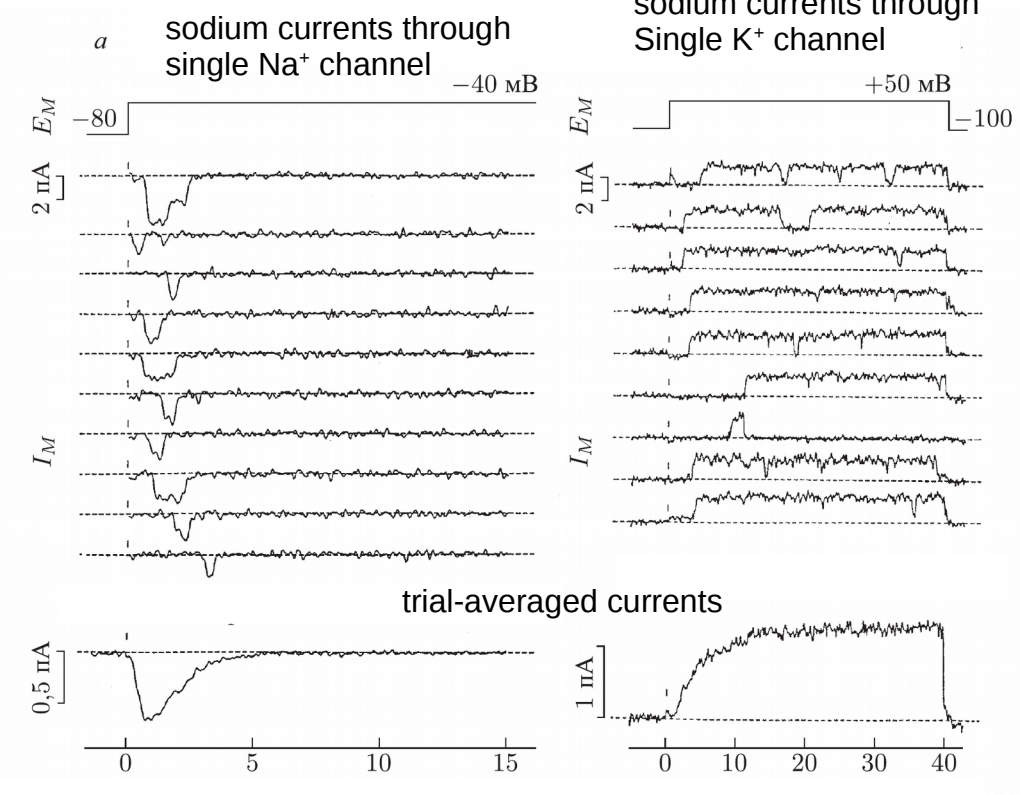
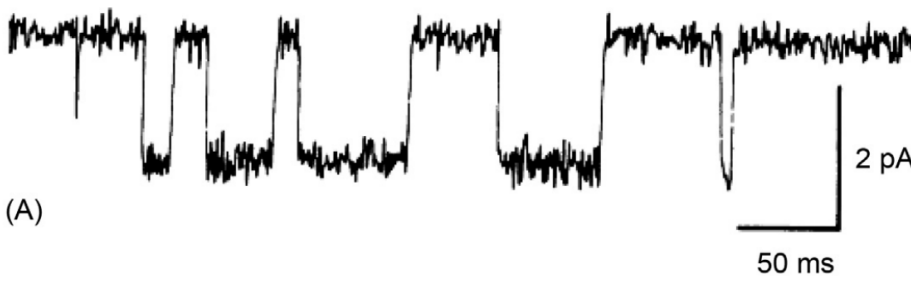
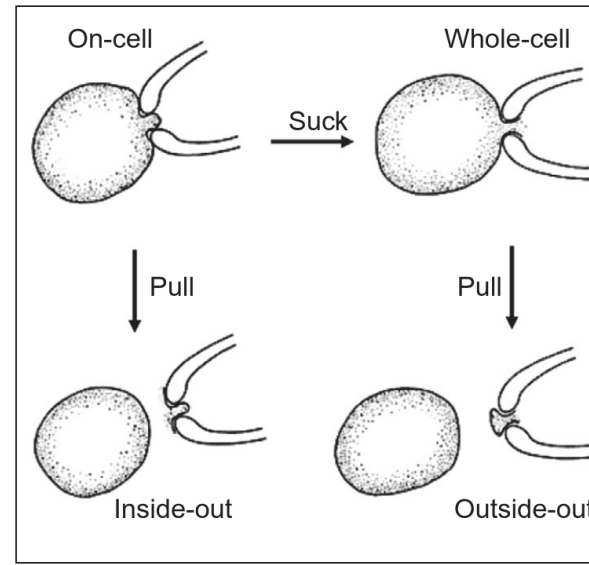
I-V relations in the GHK and linear approximations

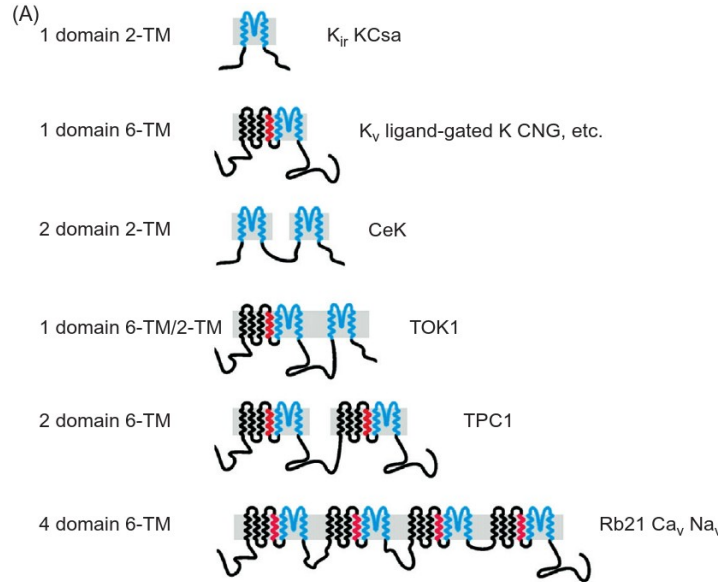


- current “rectification” — conductance in one direction is higher than in the other
- the higher difference in concentrations, the more nonlinear the curve

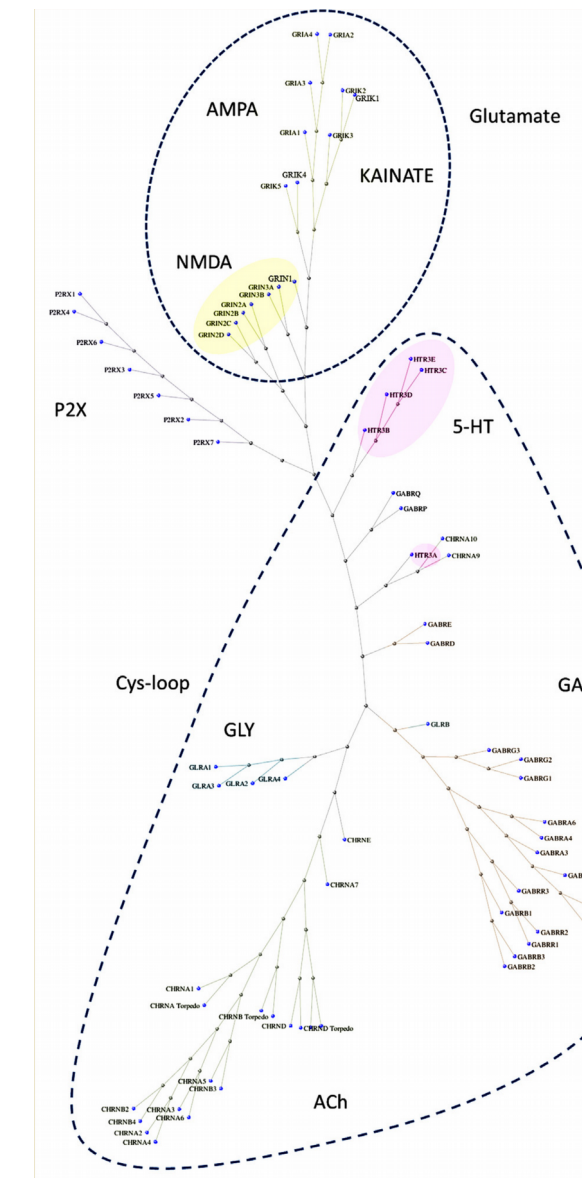
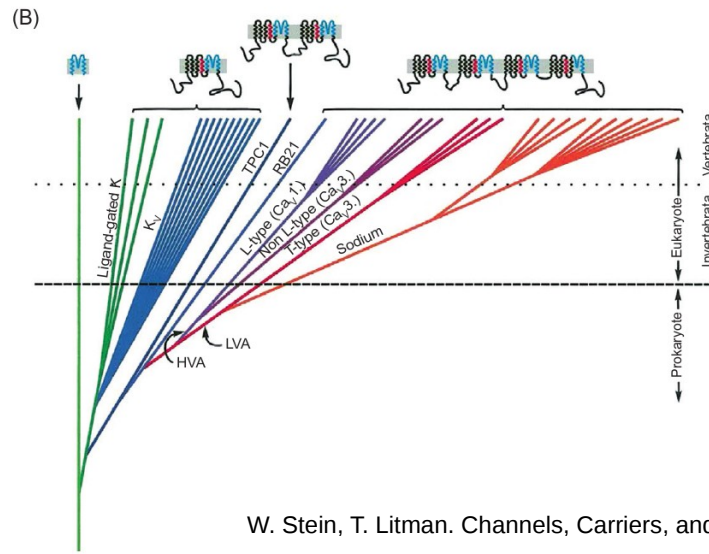


Ion channels

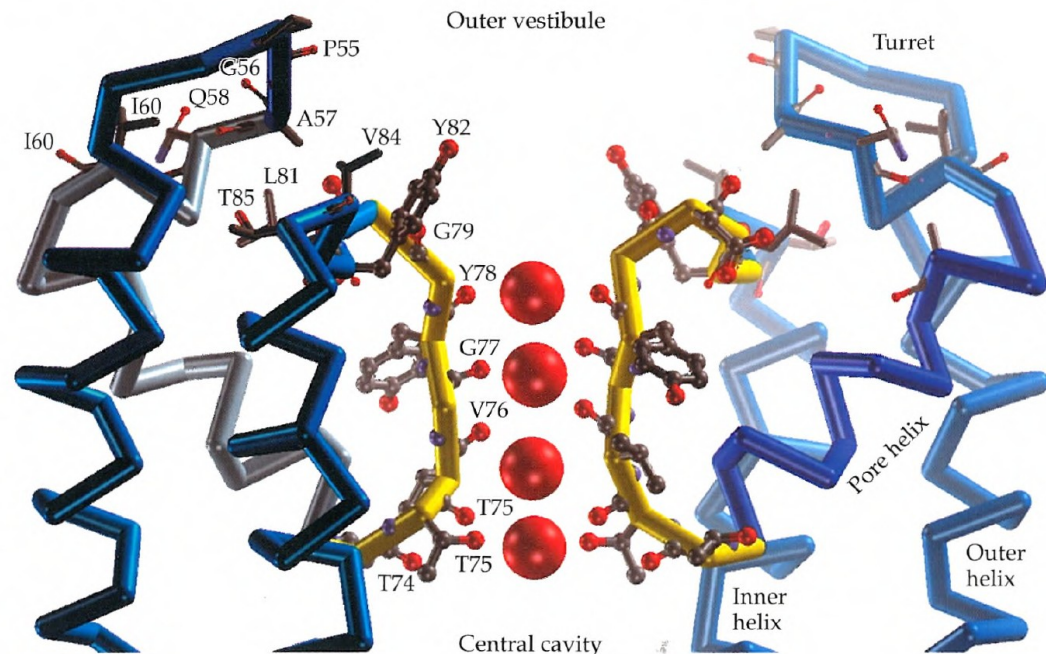
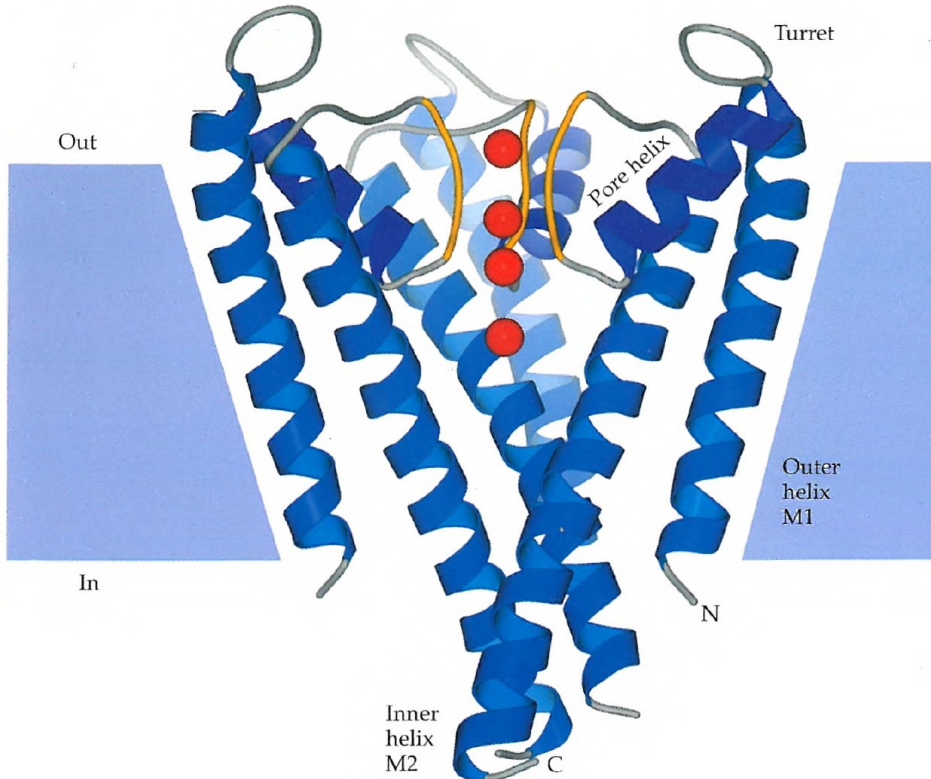




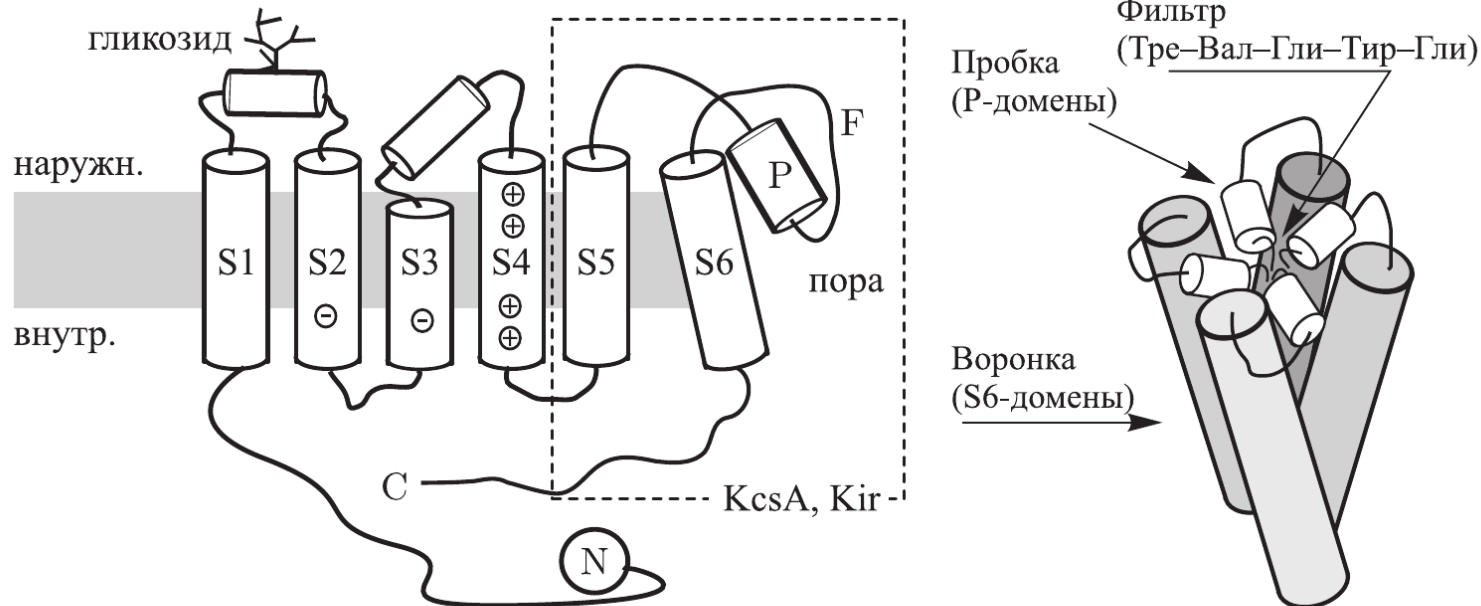
Channel families



Voltage-gated K⁺-channels (Kv)



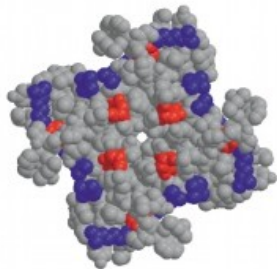
Voltage-gated potassium channels



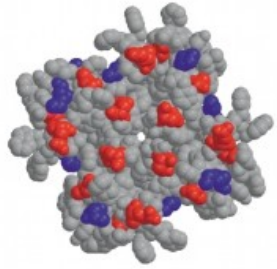
Kv-channels

Human Molecular Genetics, 2002, Vol. 11, No. 20 2427

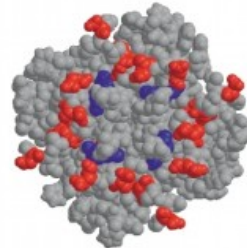
acidic residues
basic residues



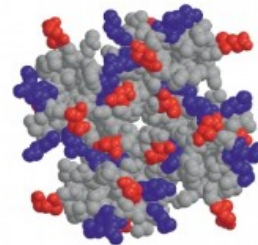
KcsA



Shak



Kir6.2



GluR0

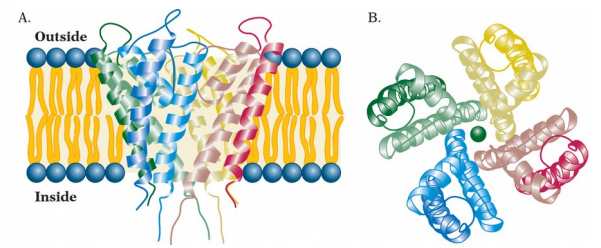
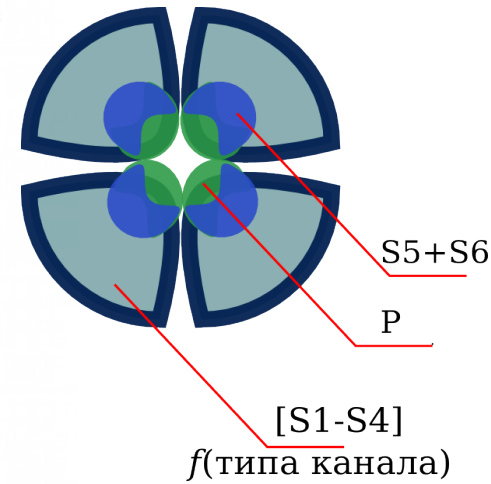
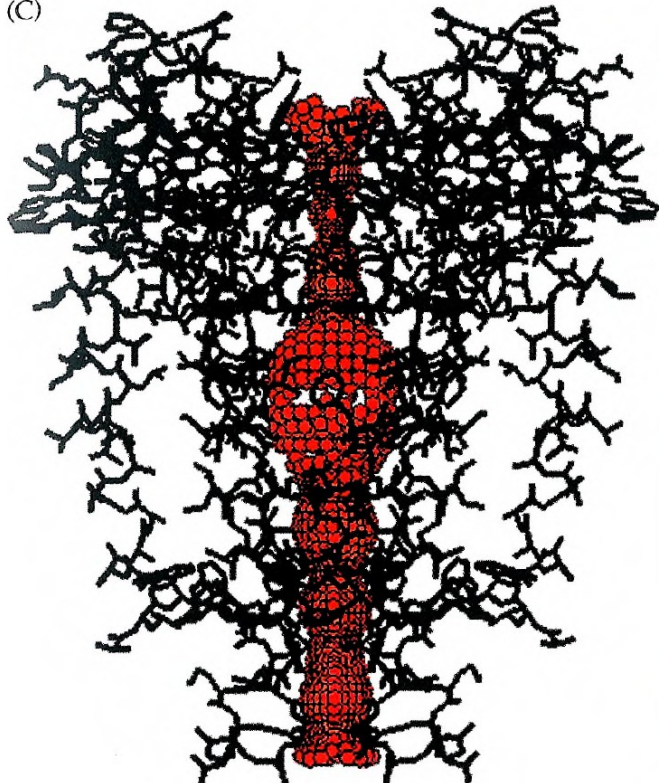


Figure 2. K-channel homology models: KcsA, Shaker, Kir6.2 and GluR0. Each model is viewed from the filter-end mouth (i.e. the extracellular mouth for the K channels and the intracellular mouth for GluR0) down the pore. Acidic residues are coloured red, basic blue and others grey.

The central cavity

296

(C)



(D)

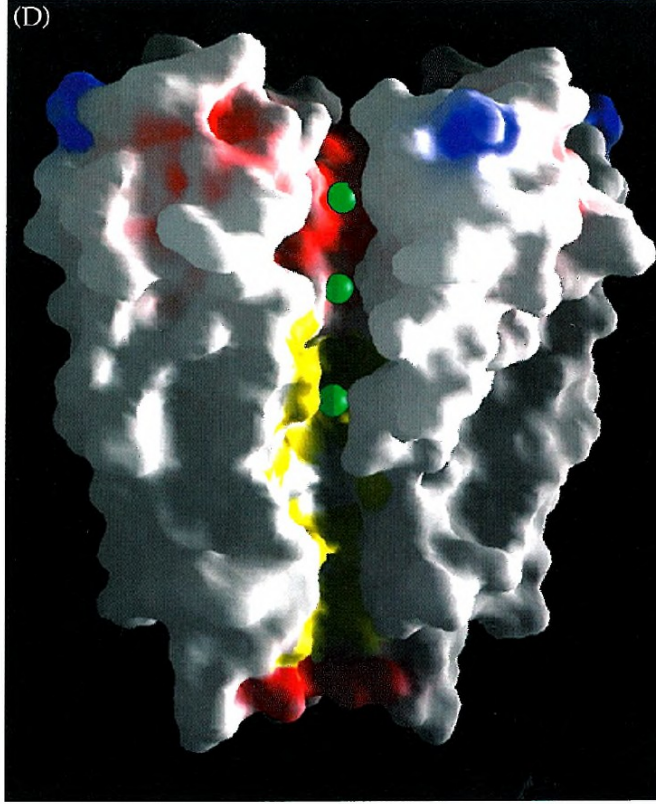
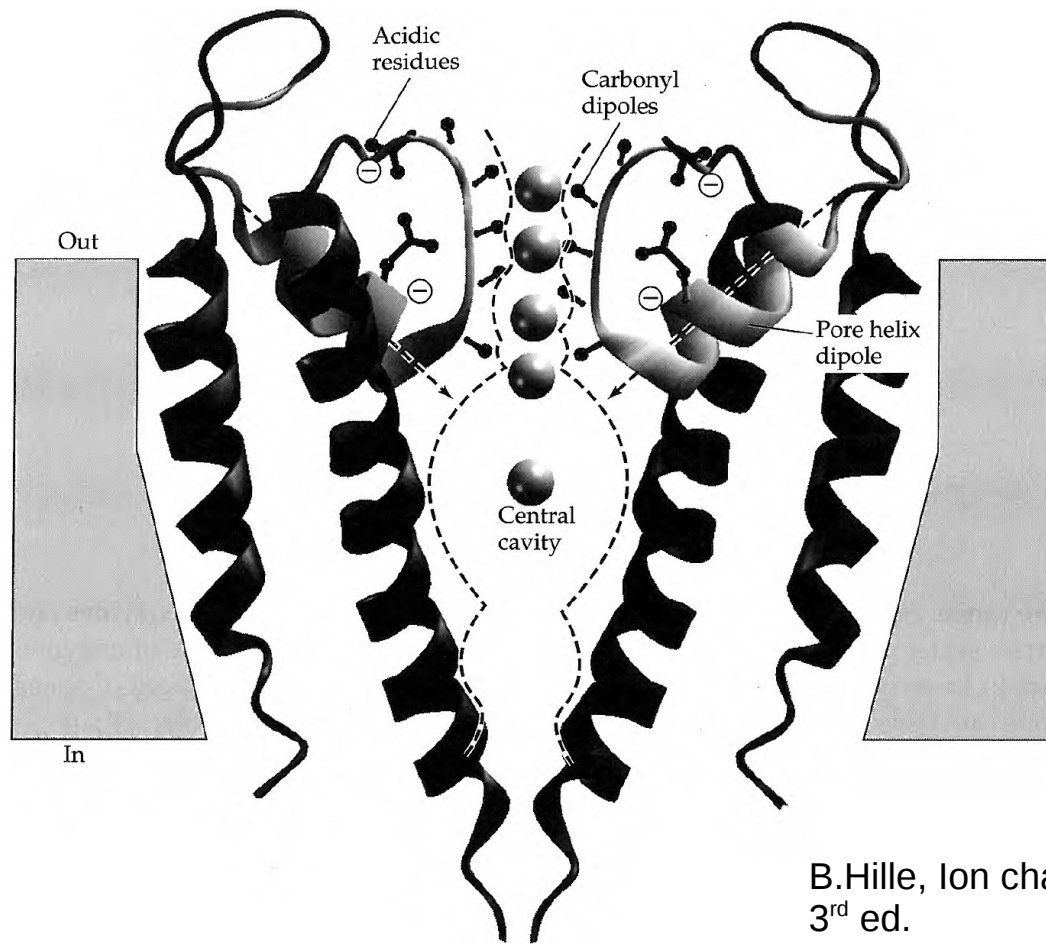


Fig. 2. KcsA fold and backbone atoms of the selectivity filter are shown in ball-and-stick format. The lipid bilayer is indicated by the horizontal dotted lines. IC = intracellular; EC = extracellular. (B) The pore-lining surface of KcsA (calculated using HOLE [107,108]) aligned with the fold diagram in (A) and showing the filter (F), cavity (C) and gate (G) regions. Diagrams generated using VMD [109] and Povray.

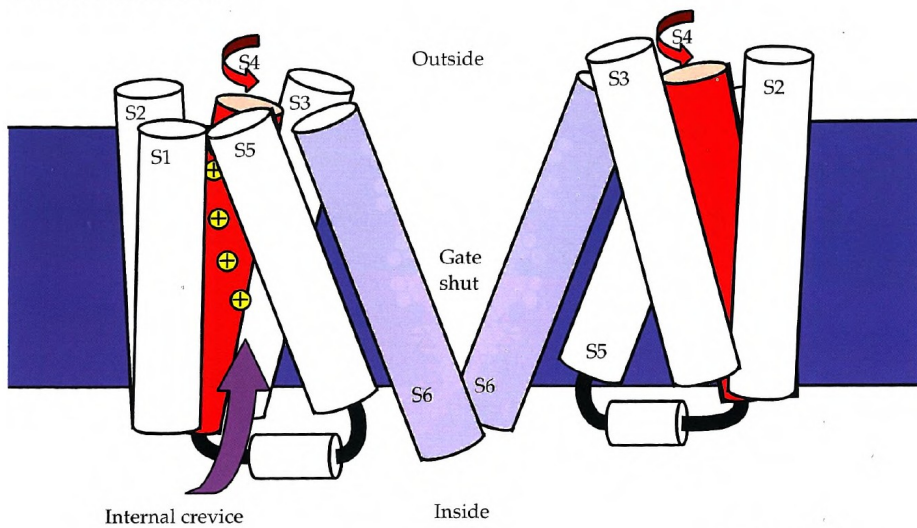
Ion stabilization in the pore



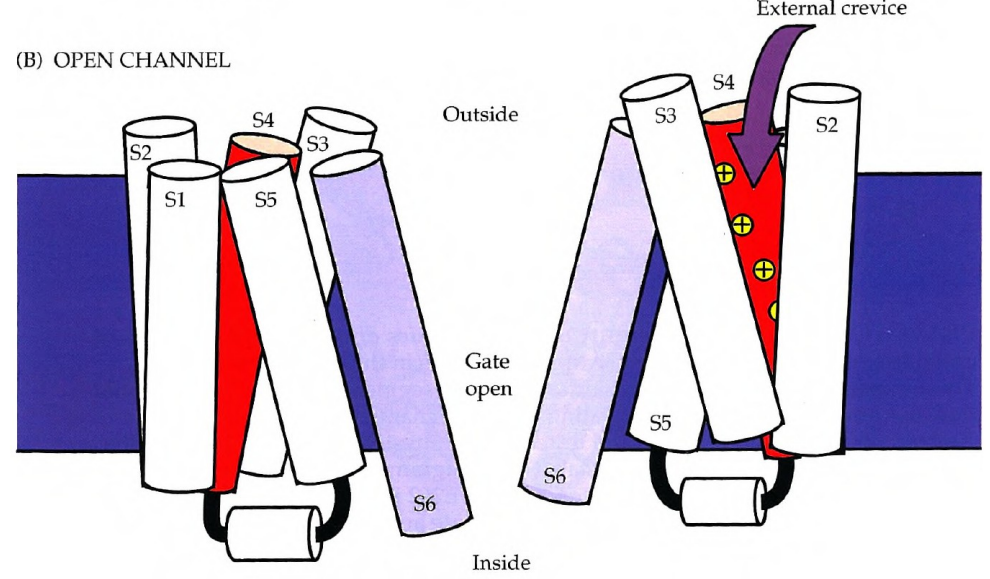
B.Hille, Ion channels of excitable membranes
3rd ed.

Channel gating

(A) CLOSED CHANNEL



(B) OPEN CHANNEL



Channel gating

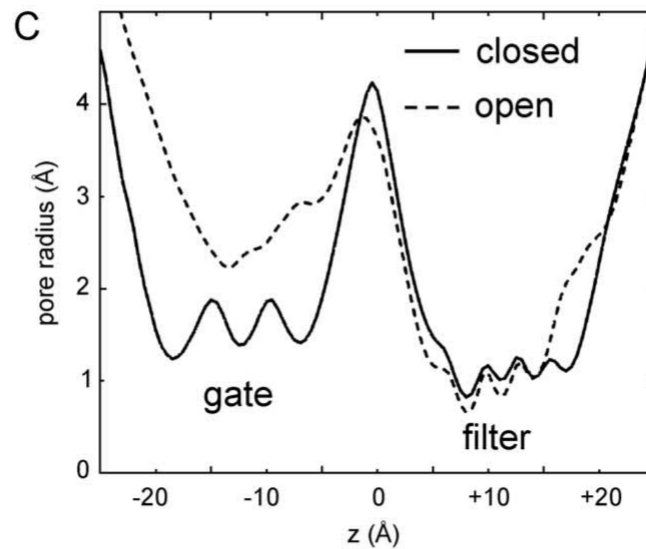
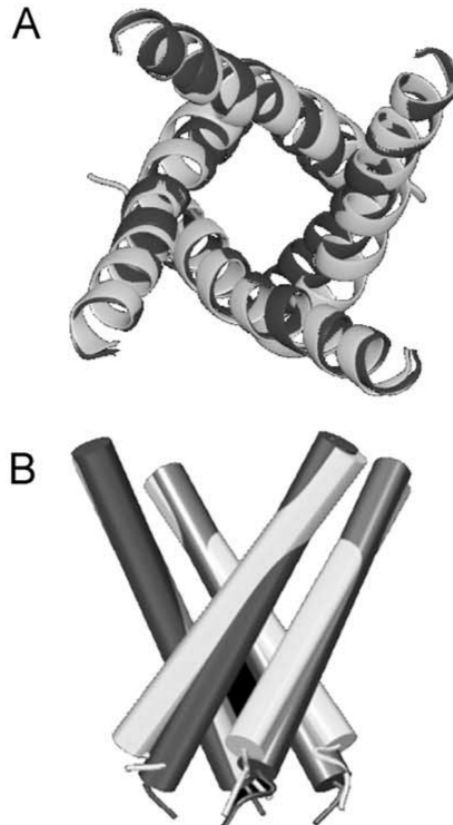
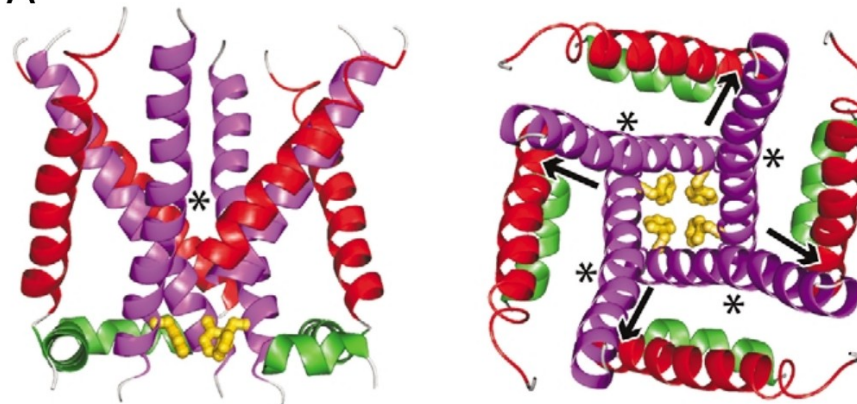


Fig. 8. Modelling the open state of KcsA. The two upper diagrams show a superimposition of the M2 helices from the closed structure (dark grey) and an open state model (light grey) of KcsA. (A) View looking down the pore axis from the filter towards the intracellular mouth of the channel. (B) View down a perpendicular to the pore axis, the extracellular (filter) end of the helices at the top and the intracellular (gate) end of the helices at the bottom. (C) Pore radius profiles for closed (solid line) and open (broken line) state models of the KcsA channel. Both profiles are averages derived from simulations (see Ref. [61] for details).

Channel gating

A



Б



Doyle, Trends Neurosci, 2004 Jun;27(6):298-302.

Glutamate receptors that make channels

Ionotropic glutamate receptors (iGluRs)				
AMPARs	KainateRs	NMDARs	DeltaRs	
GluA1	GluK1 GluK4	GluN1* GluN2A GluN3A*	GluD1	GluD2*
GluA2	GluK2 GluK5	GluN2B GluN3B*		
GluA3	GluK3	GluN2C		
GluA4		GluN2D		

- heterotetrameres
- pre- and post-translational modifications

Molecular structure of Glu-receptors

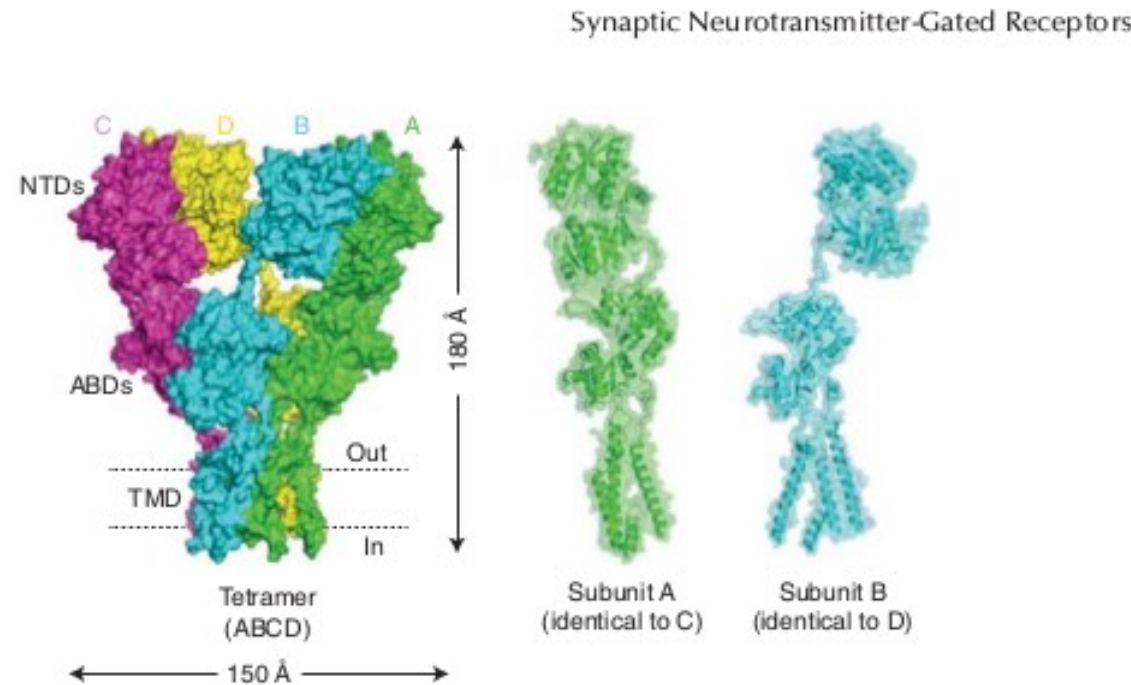
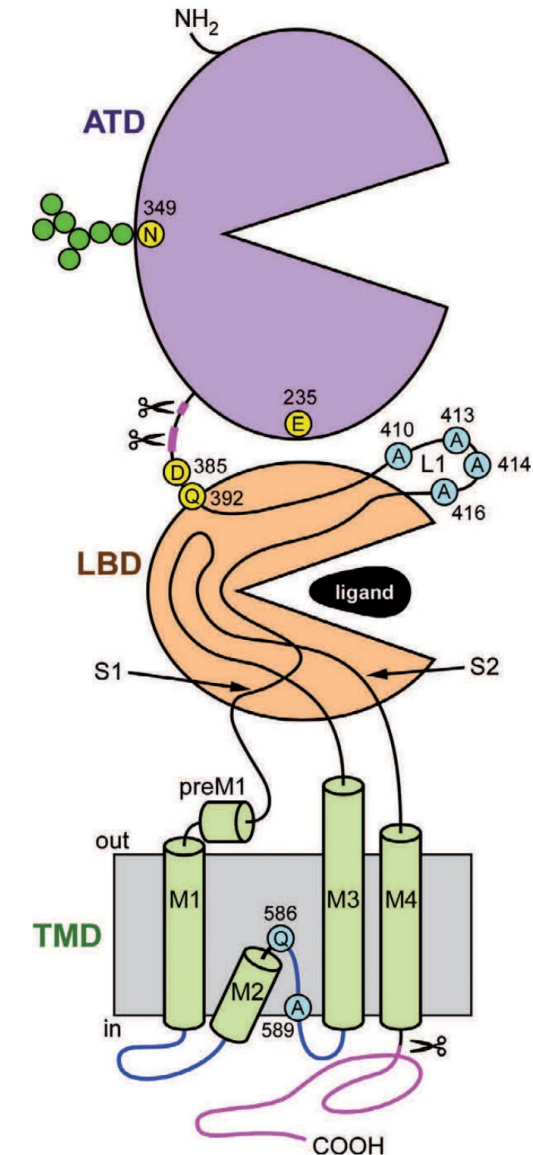


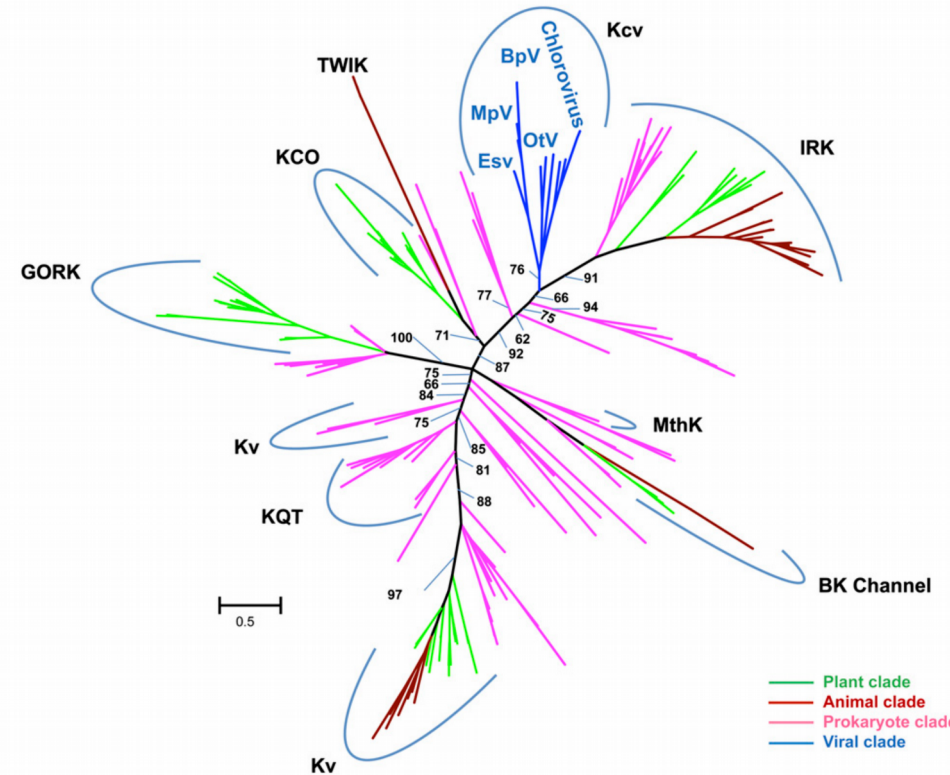
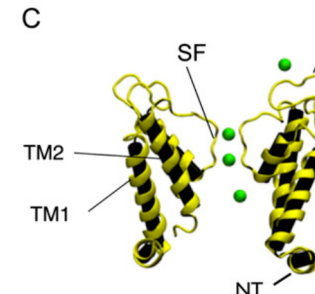
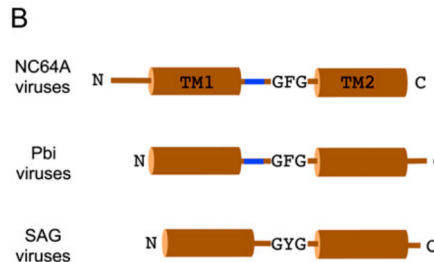
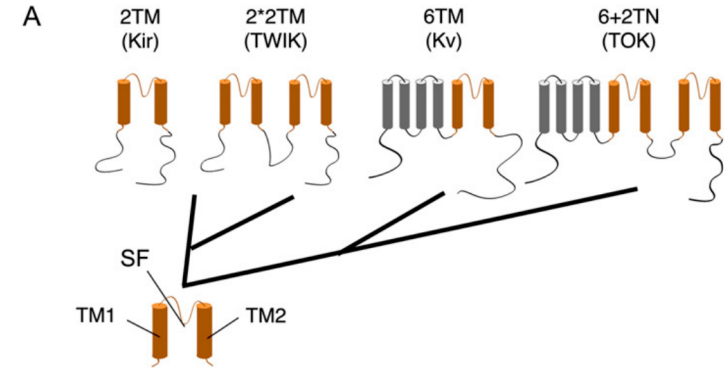
Figure 6. The tetrameric structure of the AMPA GluA2 receptor. (Left) X-ray crystal structure of the AMPA GluA2 homotetrameric receptor (Sobolevsky et al. 2009). Each subunit is in a different color. The tetramer shows a typical layer organization with at the “top” the amino-terminal domains (ATDs or NTDs), at the “bottom” the transmembrane domain (TMD) where the ion channel sits, and sandwiched between the two the agonist-binding domains (ABDs or S1S2 domains) binding glutamate (or glycine/d-serine). (Right) Subunit non-equivalence. α -Carbon traces of subunit A and subunit B with the ABDs similarly oriented. Note the striking difference in overall domain orientation between the two subunits.



Potassium Ion Channels: Could They Have Evolved from Viruses?^{1[W]}

Plant Physiol. Vol. 162, 2013

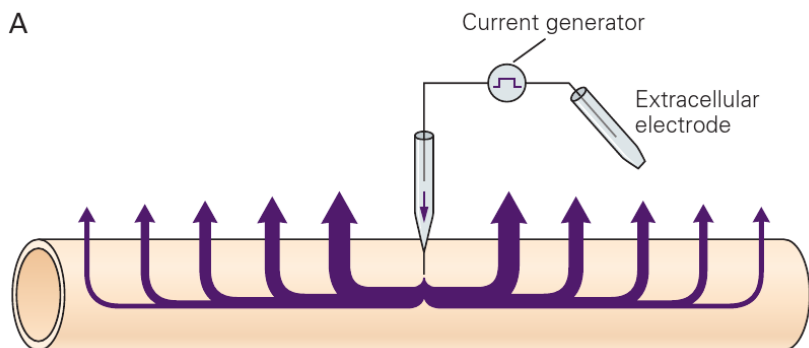
Gerhard Thiel*, Anna Moroni, Guillaume Blanc, and James L. Van Etten



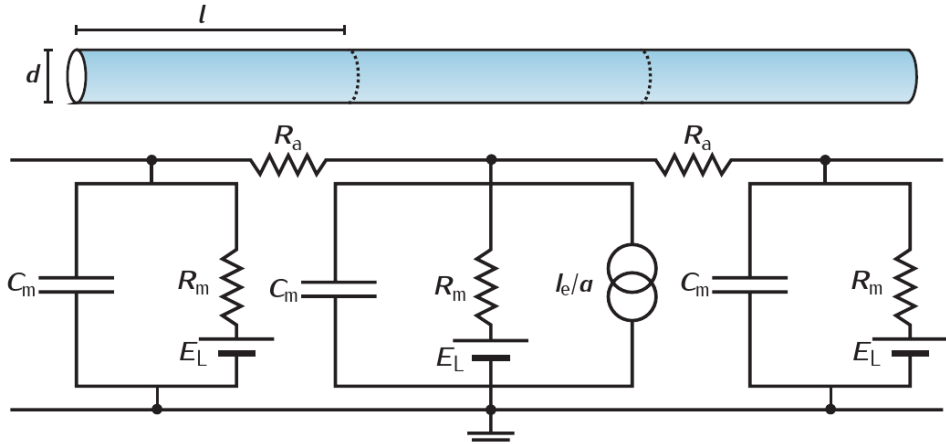
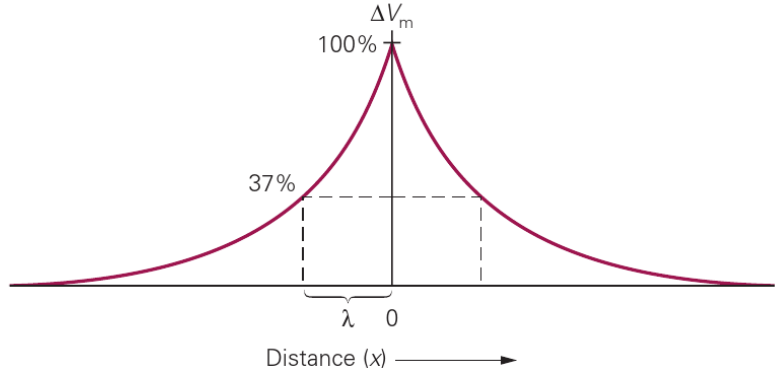
. It is not our intent in this review to resolve the controversy about the evolutionary origin of large dsDNA viruses but to explore the possibility that some large dsDNA viruses that infect eukaryotic algae encode a K^+ channel protein that might be the evolutionary ancestor of all K^+ channel proteins.

Cable properties of the nerve fibre

A



B

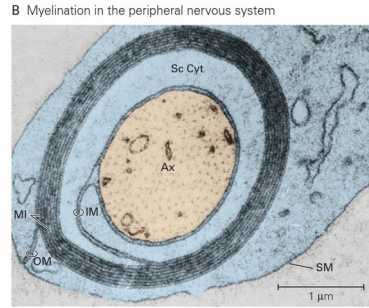
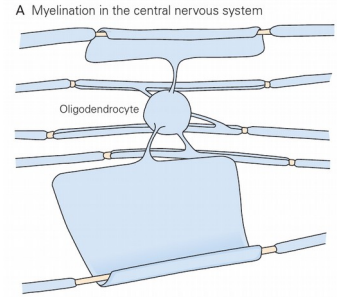


$$C_m \frac{\partial V}{\partial t} = \frac{E_m - V}{R_m} + \frac{d}{4R_a} \frac{\partial^2 V}{\partial x^2} + \frac{I_e}{\pi d}.$$

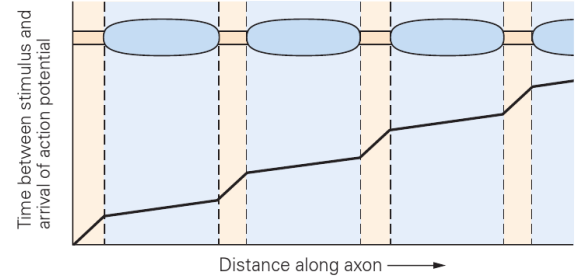
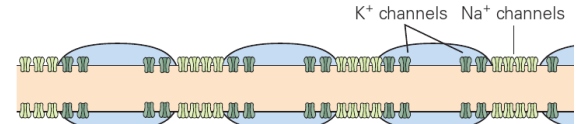
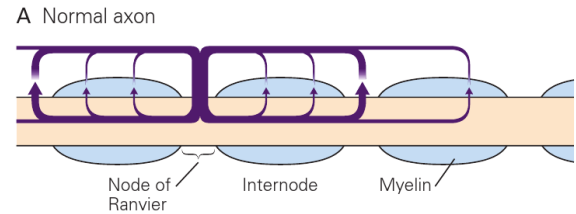
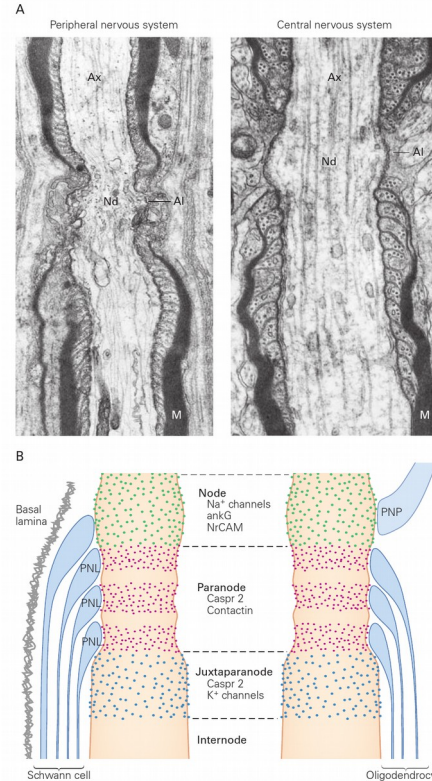
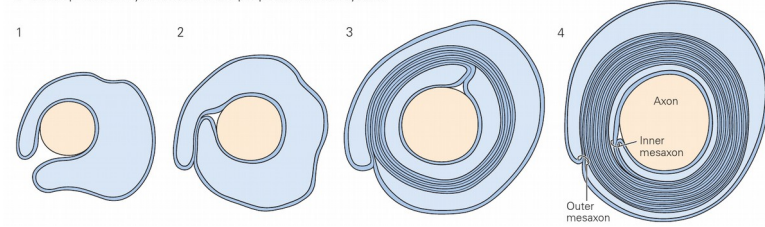
$$V(x) = E_m + R_\infty I_e e^{-x/\lambda}.$$

$$\lambda = \sqrt{\frac{R_m d}{4R_a}} = \sqrt{\frac{r_m}{r_a}}.$$

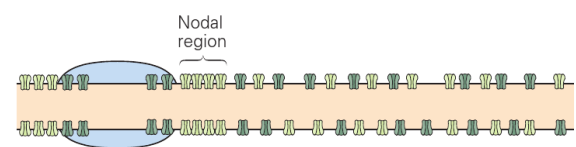
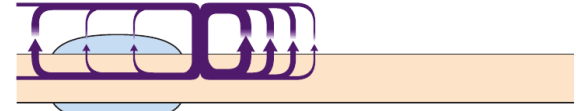
Conductance in myelinated fibres

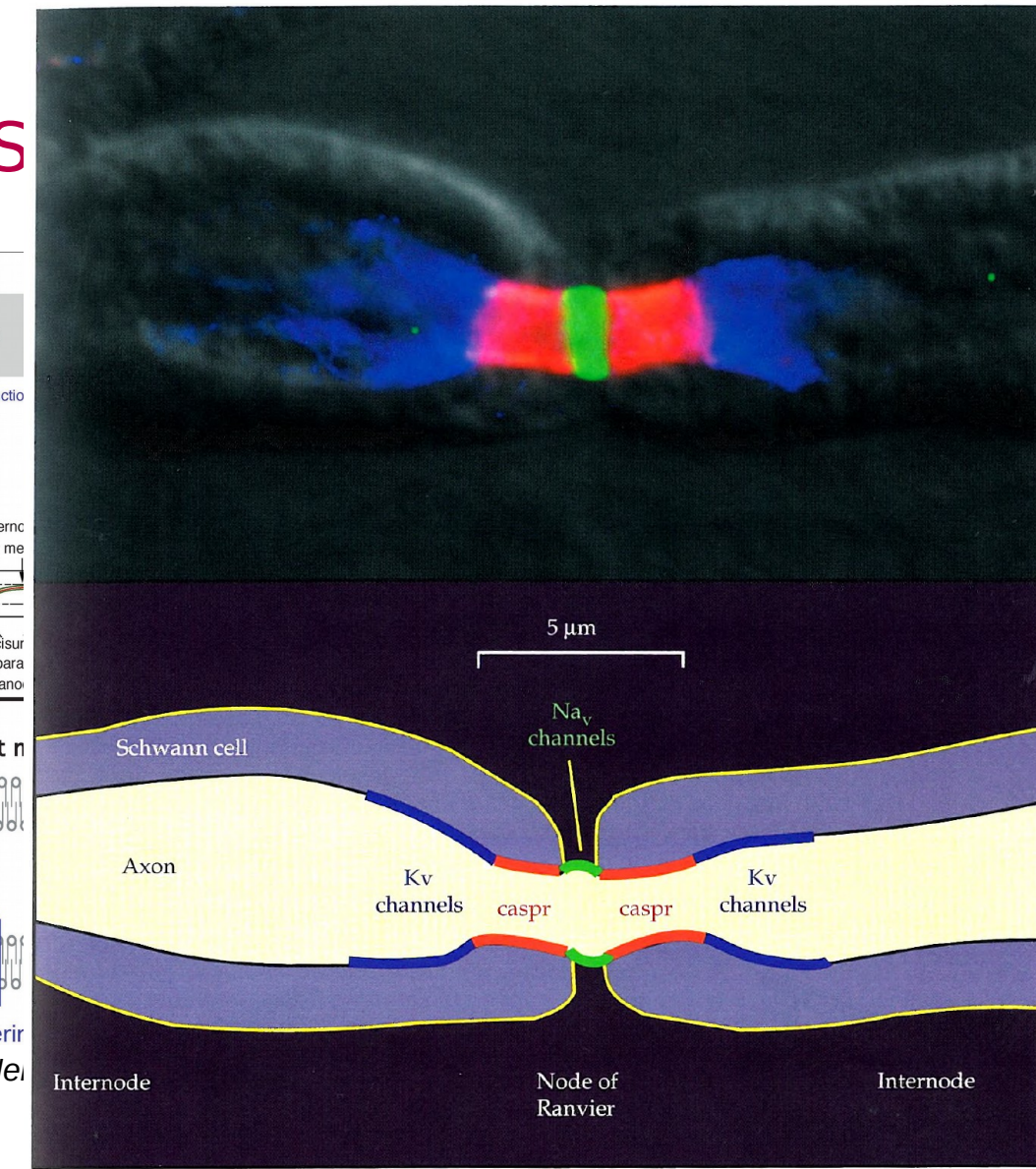


C Development of myelin sheath in the peripheral nervous system

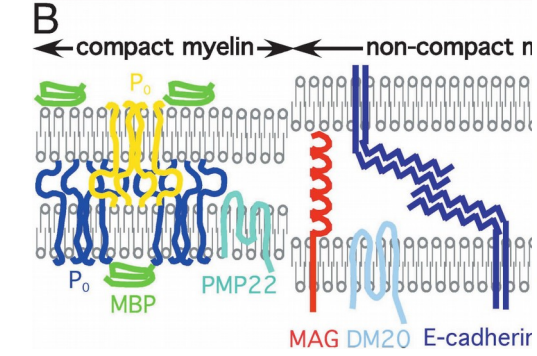
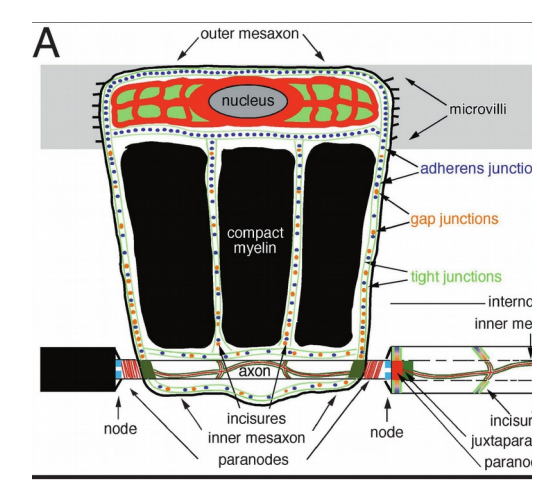


B Demyelinated axon

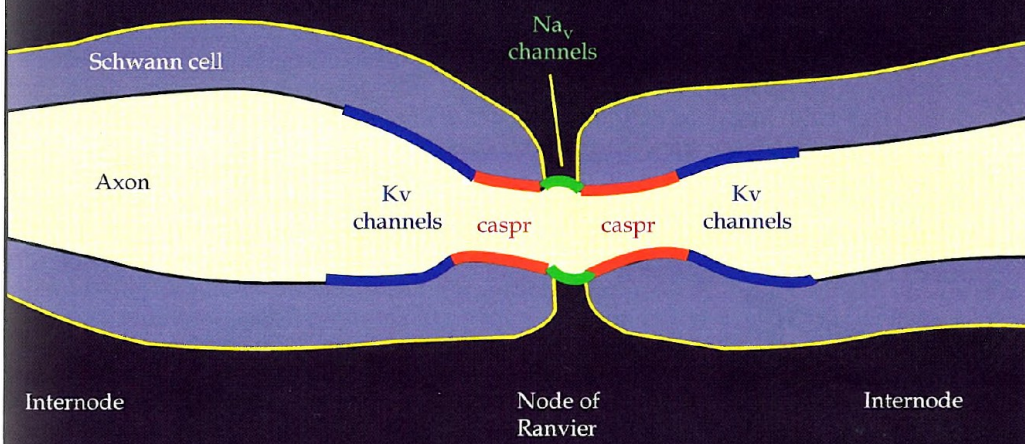




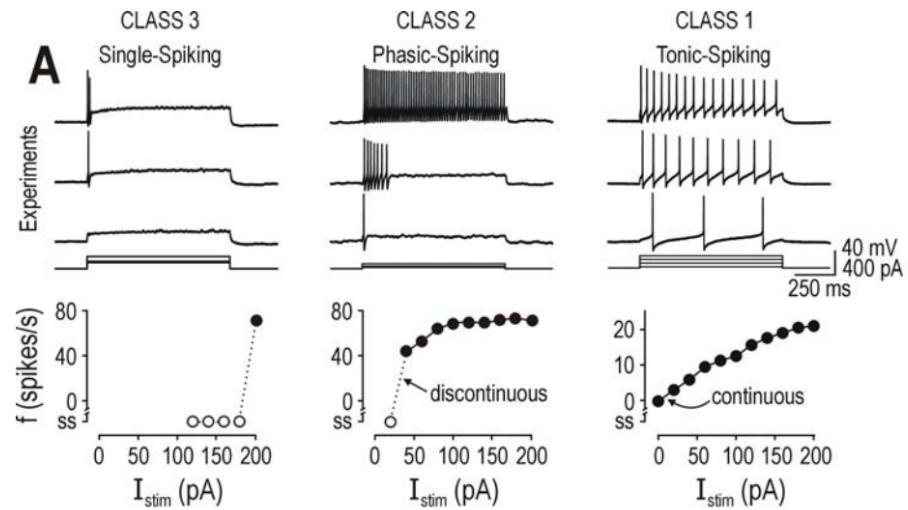
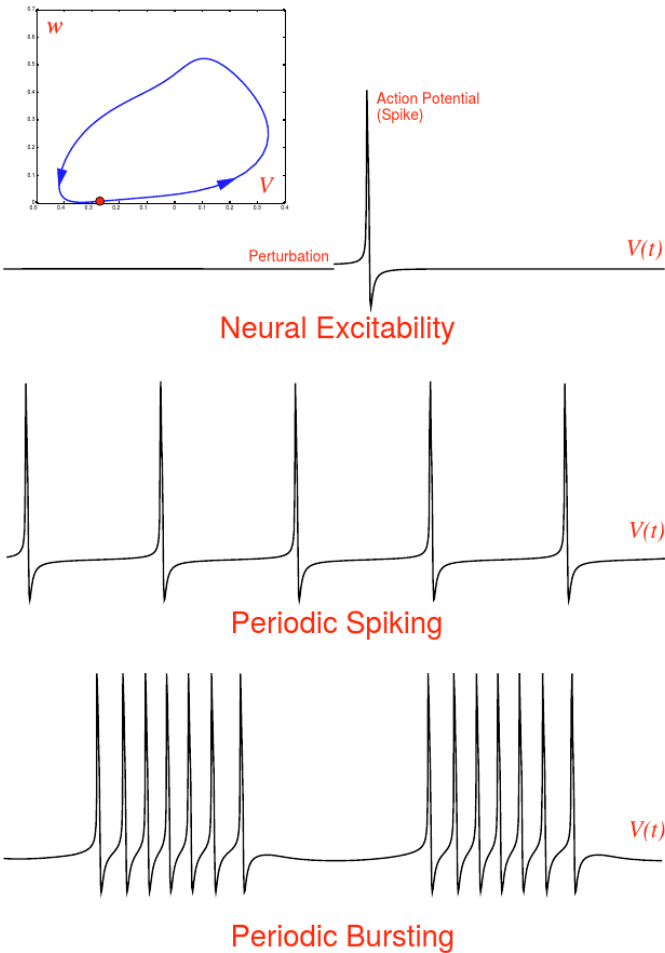
Rasband J Neurosci Res 2004



Scherer, Arroyo, J Periph Neuropathol

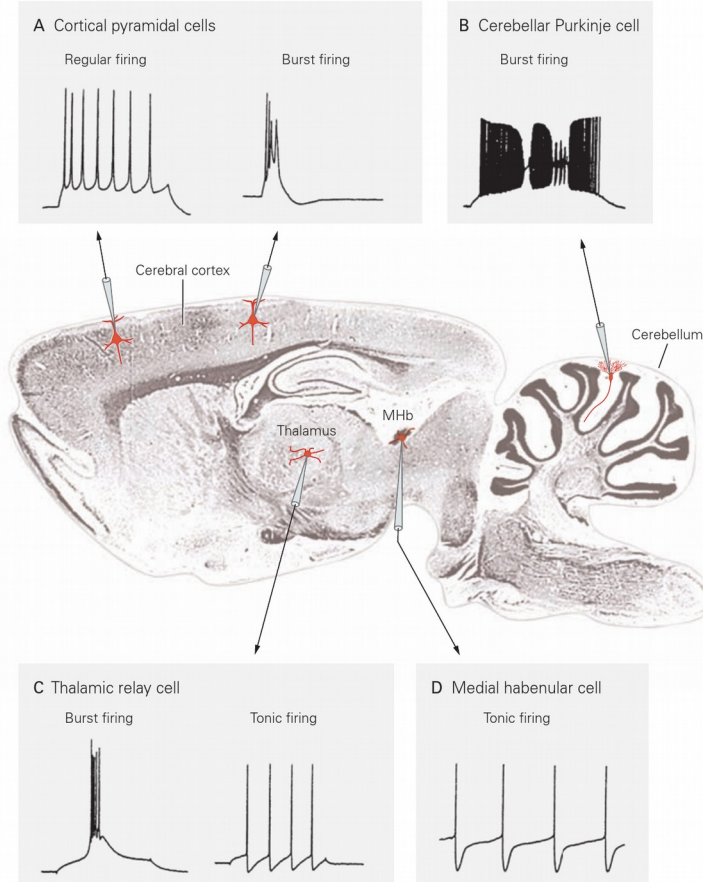
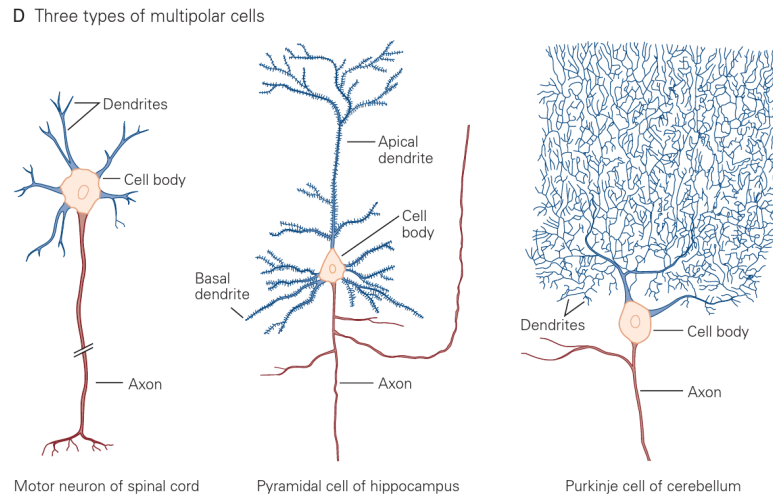
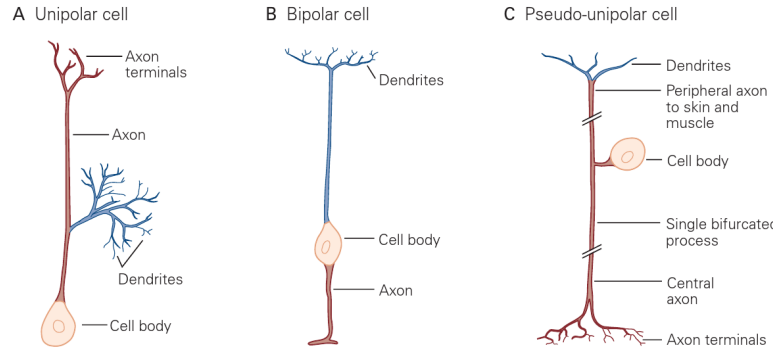


Excitability, spiking and bursting

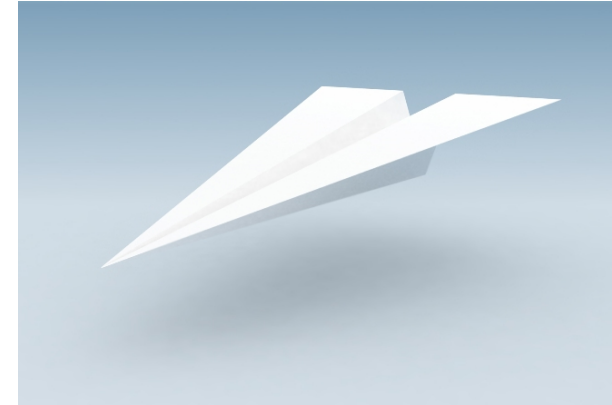


Prescott SA, De Koninck Y, Sejnowski TJ (2008)
PLoS Comput Biol 4(10): e1000198.
doi:10.1371/journal.pcbi.1000198

Different neurons have different responses to depolarizing current

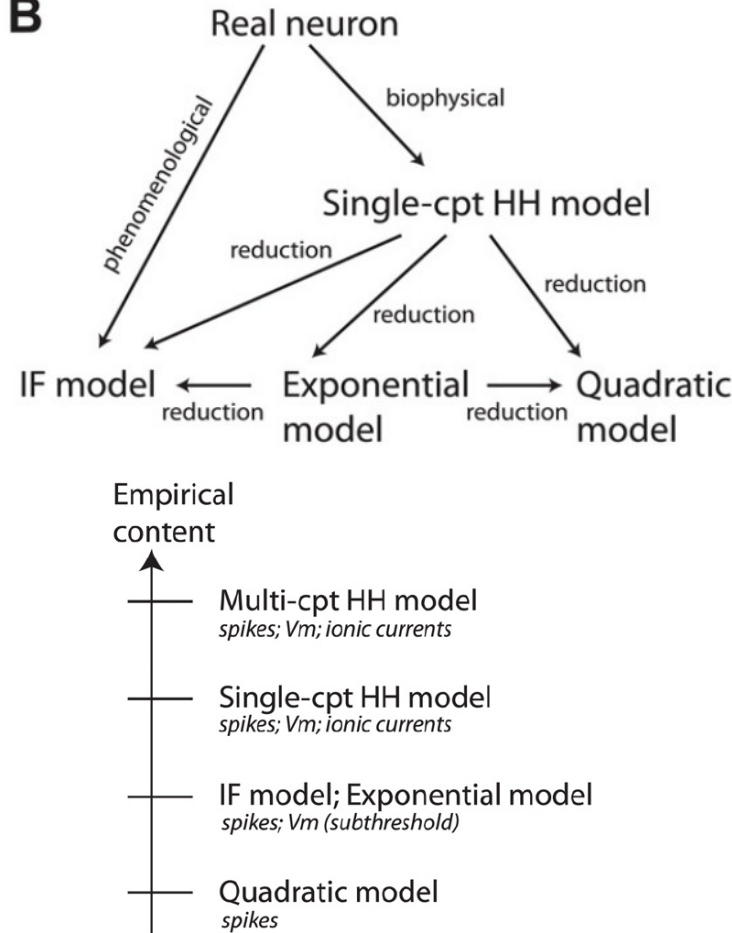


What is a good model?

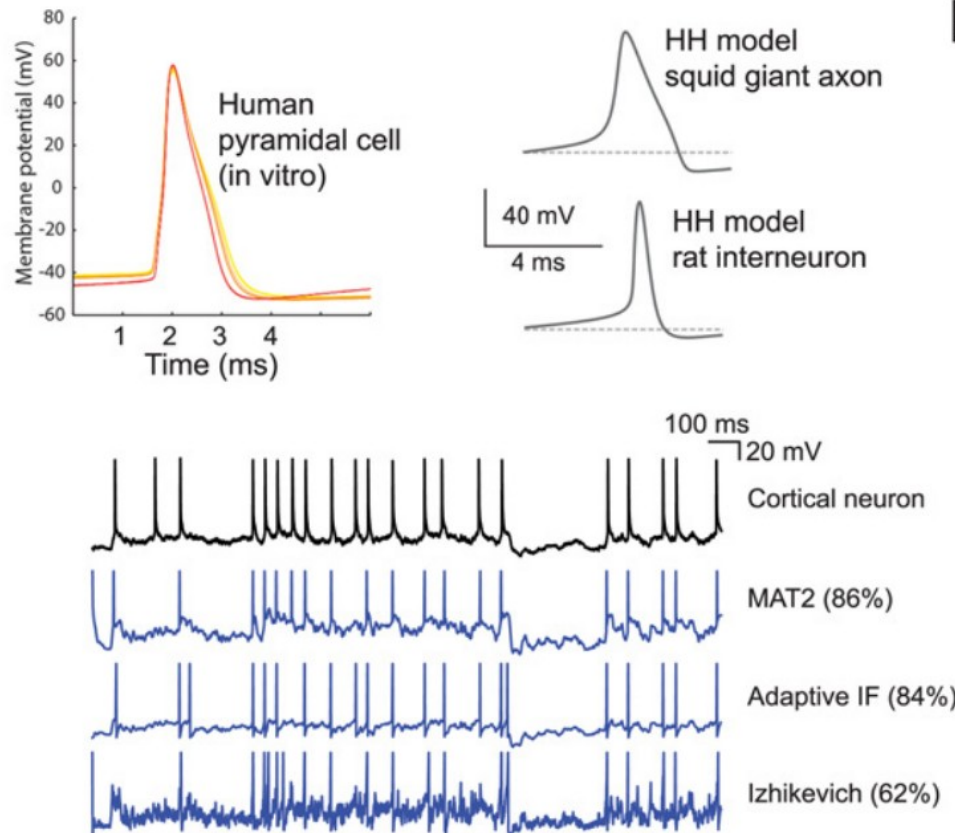


What is a good model of a neuron?

B

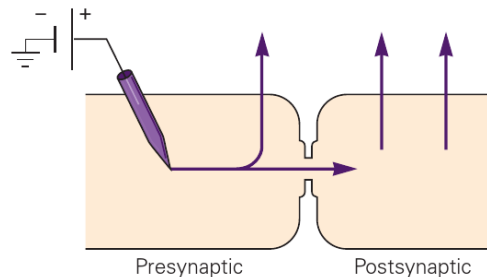


E

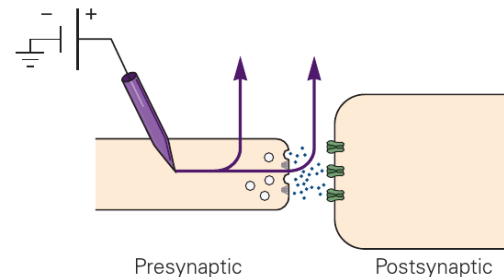


Synaptic transmission

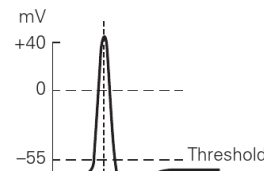
A Current pathways at electrical synapses



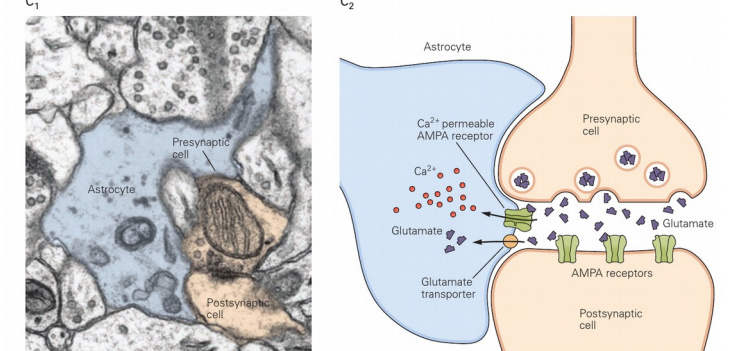
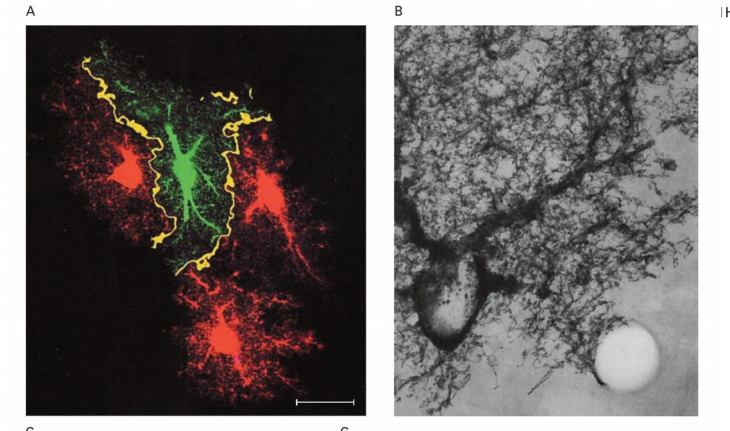
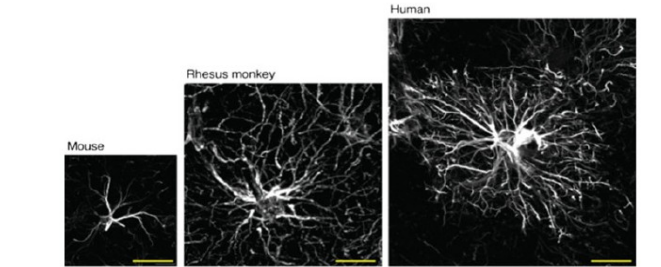
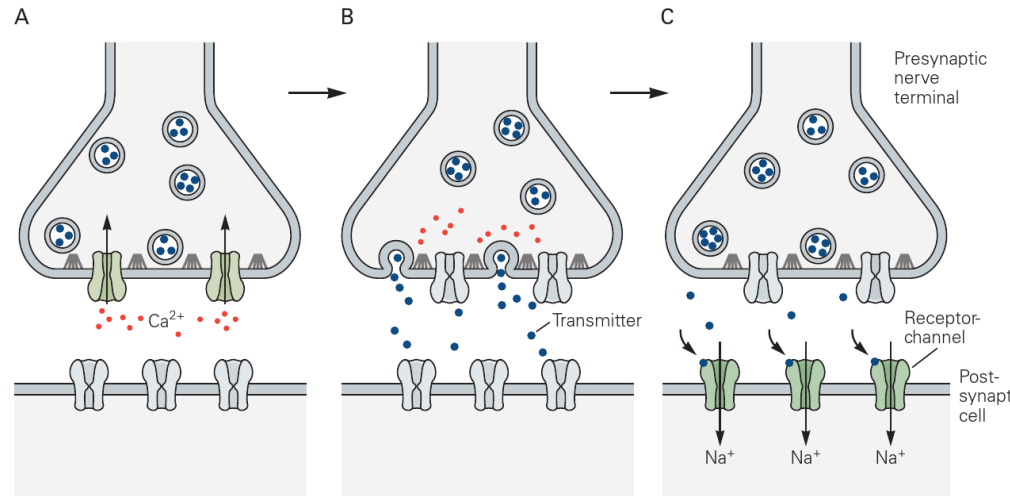
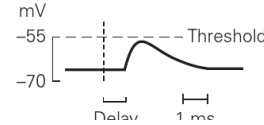
B Current pathways at chemical synapses



Presynaptic action potential

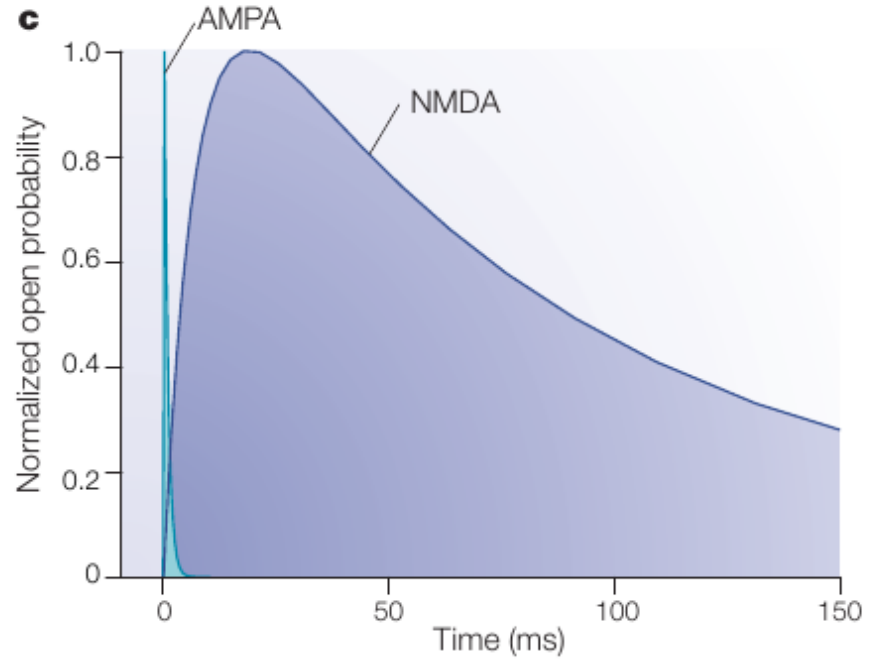
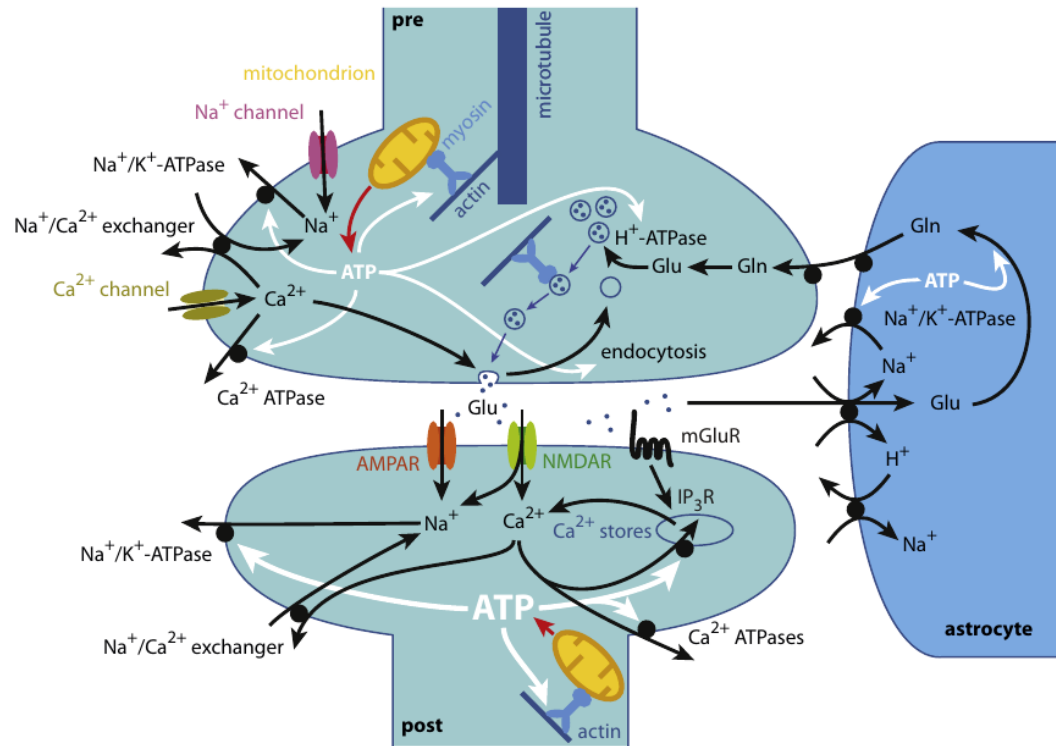


Excitatory postsynaptic potential



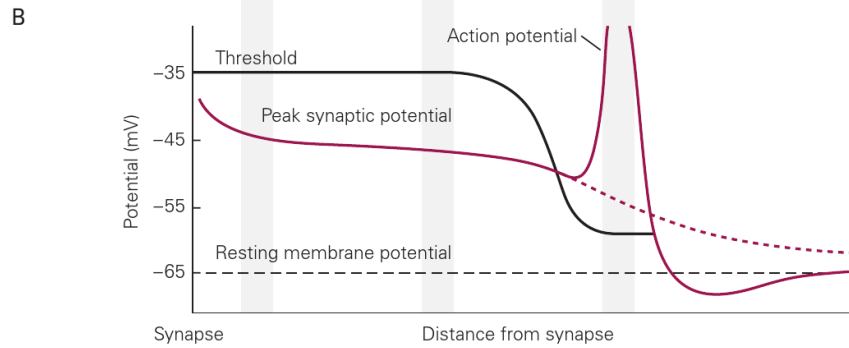
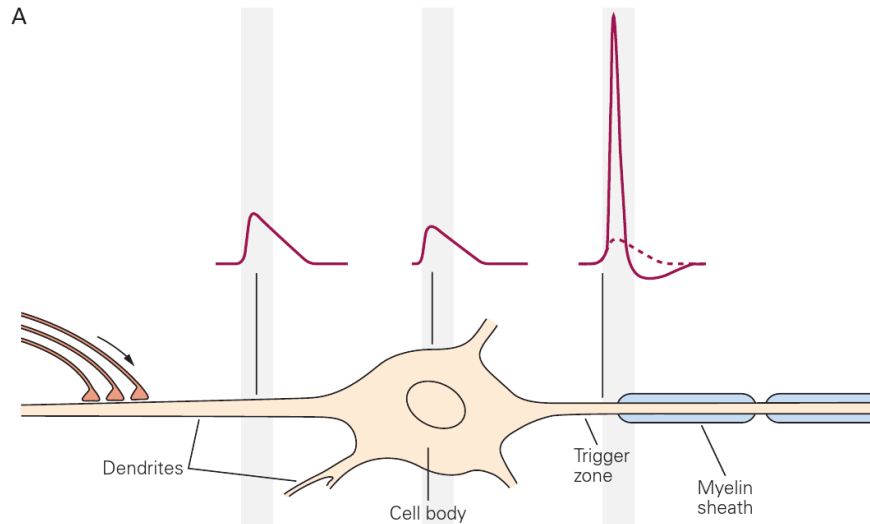
Astrocytes and the synapse ³⁴

The Glu-ergic synapse

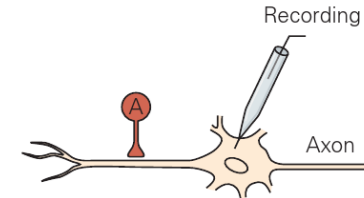


Harris, Jolivet, Attwell, 2012: doi:dx.doi.org/10.1016/j.neuron.2012.08.019

Information processing on dendrites



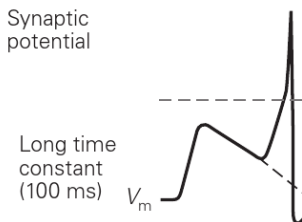
A Temporal summation



Synaptic current



Synaptic potential



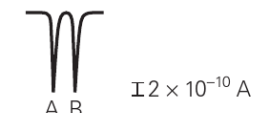
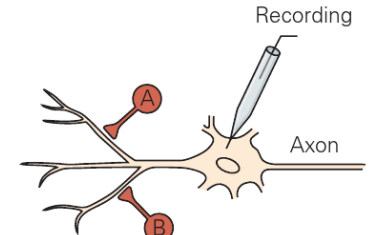
Long time constant
(100 ms)

Short time constant
(20 ms)

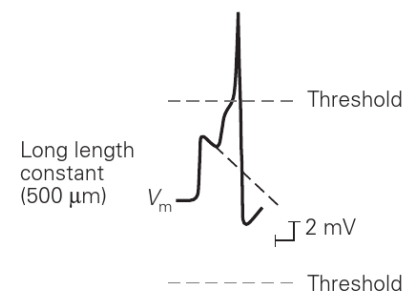
V_m

V_m

B Spatial summation



$$I \geq 2 \times 10^{-10} \text{ A}$$

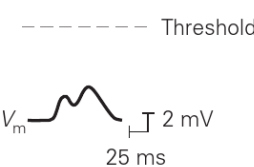


Long length constant
(500 μm)

Short length constant
(250 μm)

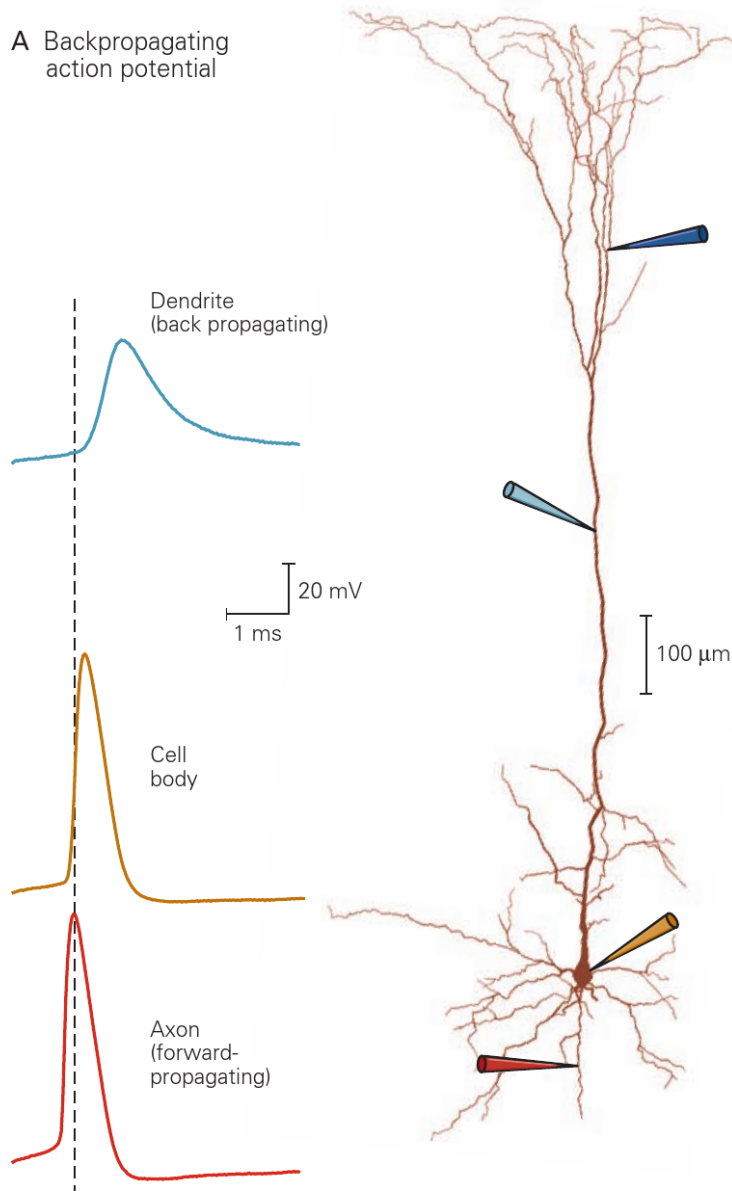
V_m

V_m

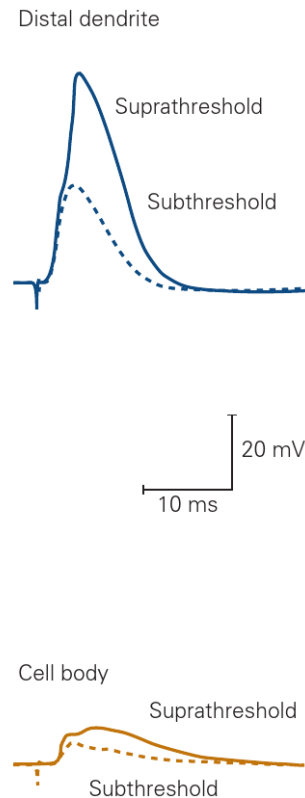


25 ms

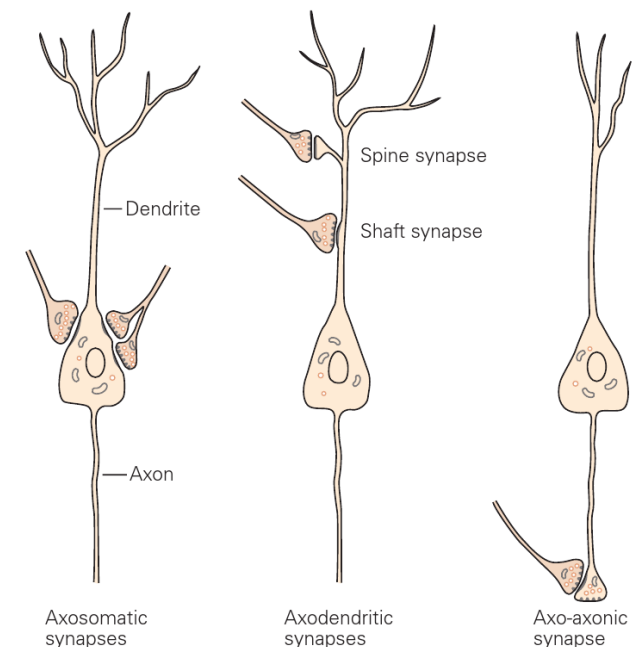
A Backpropagating action potential



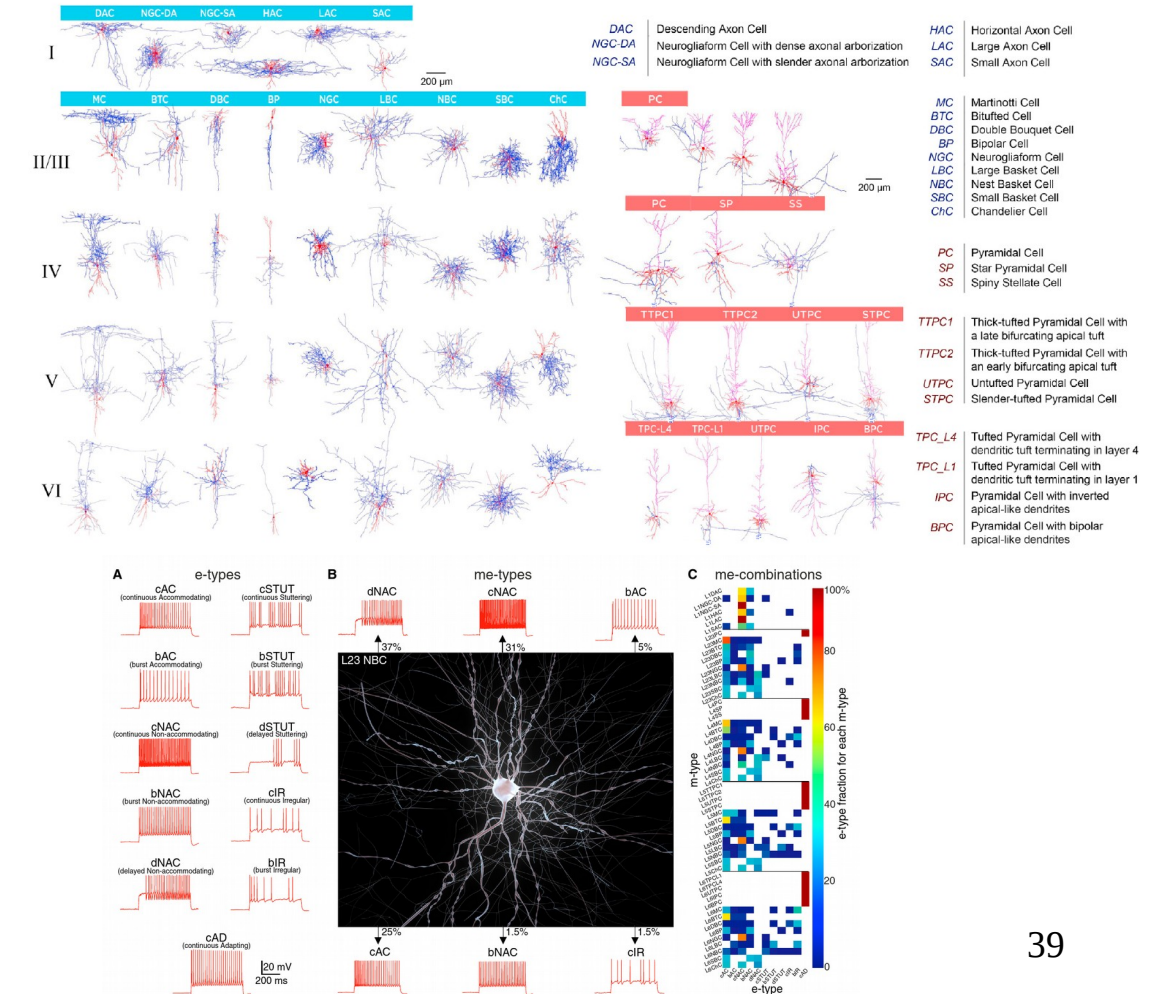
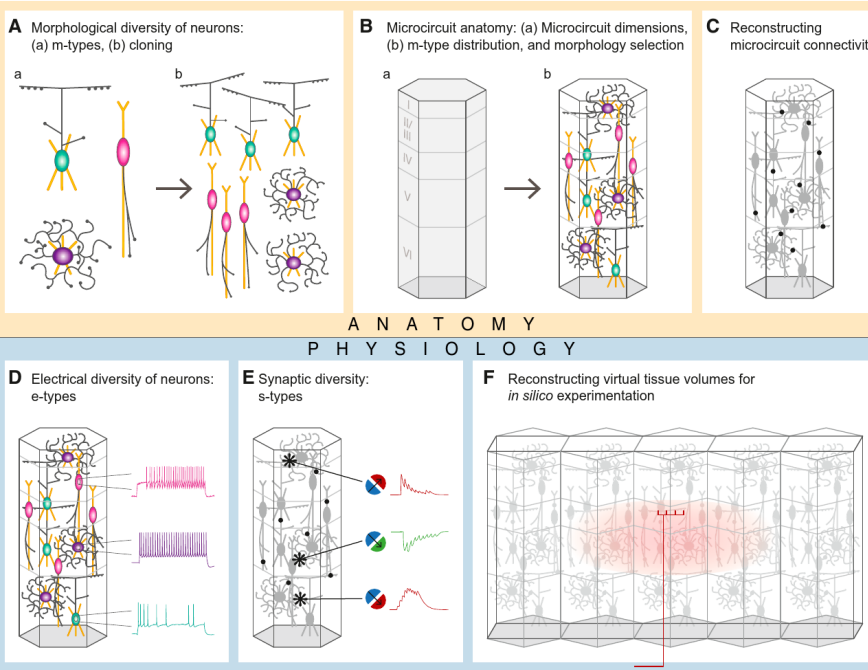
B Action potential propagating from dendrite



Spike back-propagation

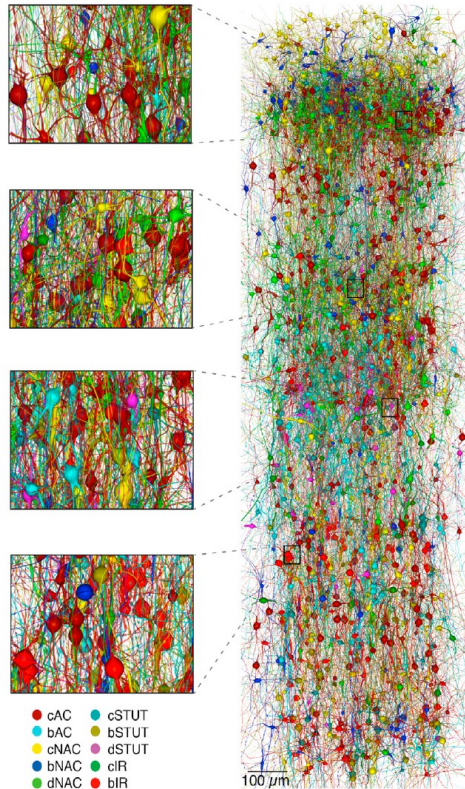


Large-scale biophysical models

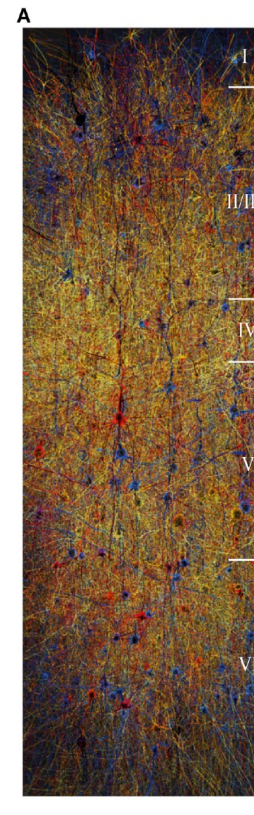
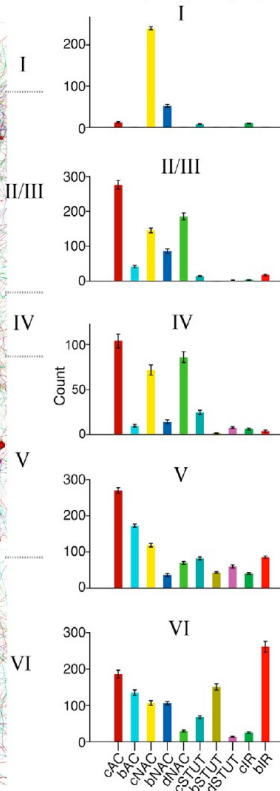


Large-scale biophysical models

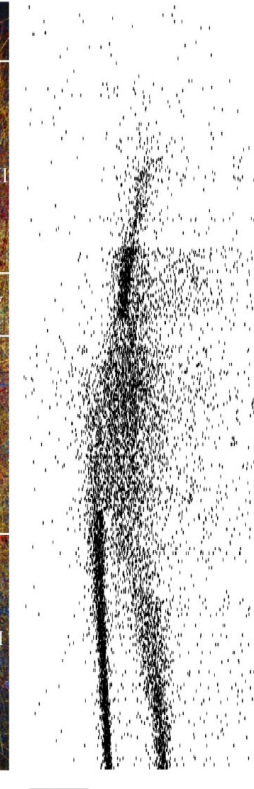
A *In silico* stain of inhibitory e-types



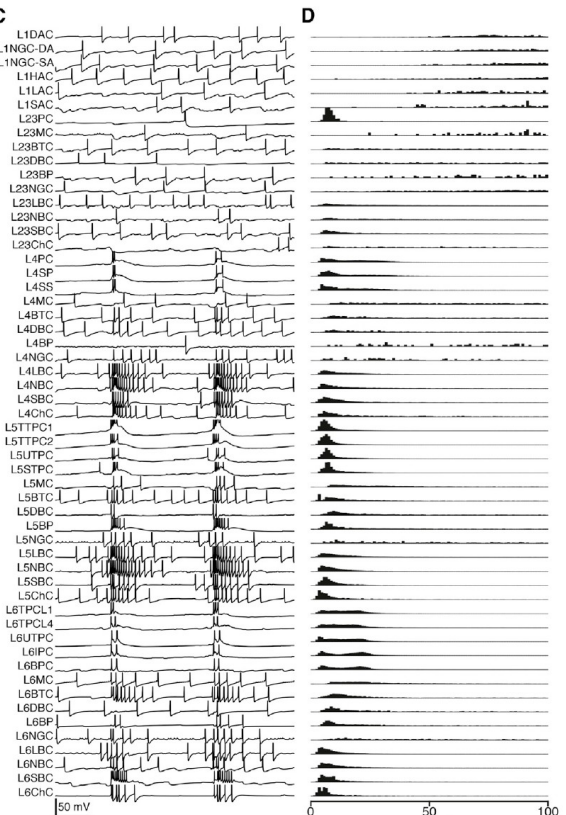
B Inhibitory e-types by layer



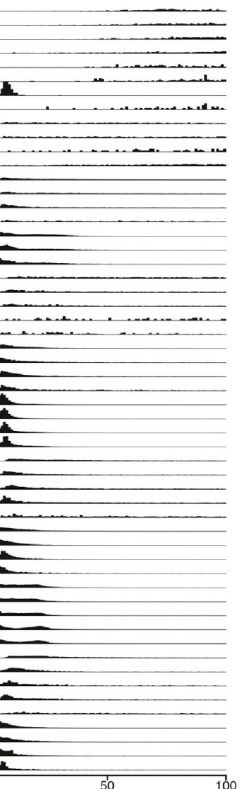
B



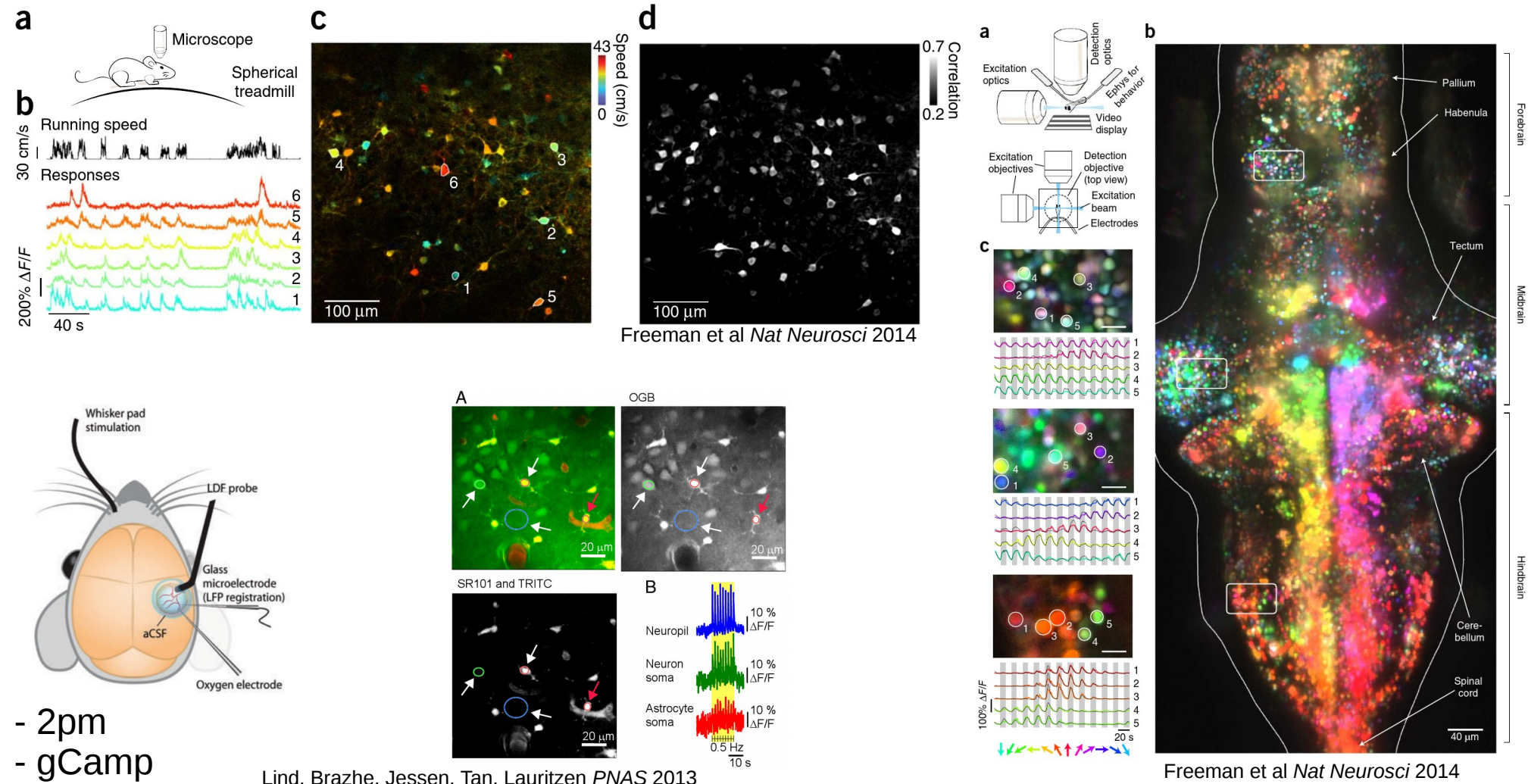
C



D



How neuronal activity is measured *in vivo*



What is measured in fMRI?

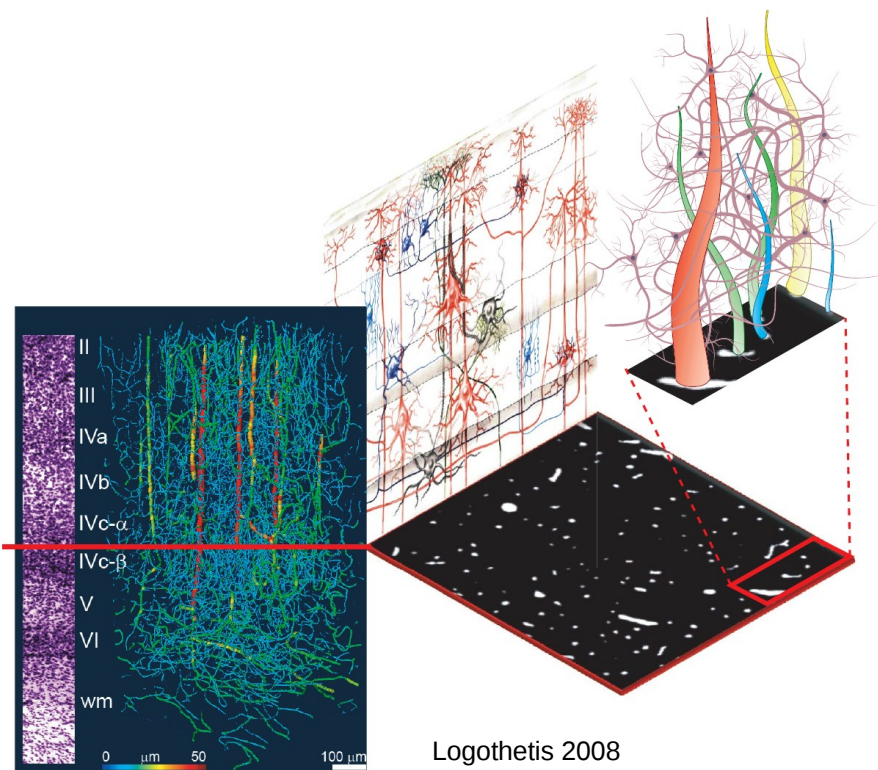
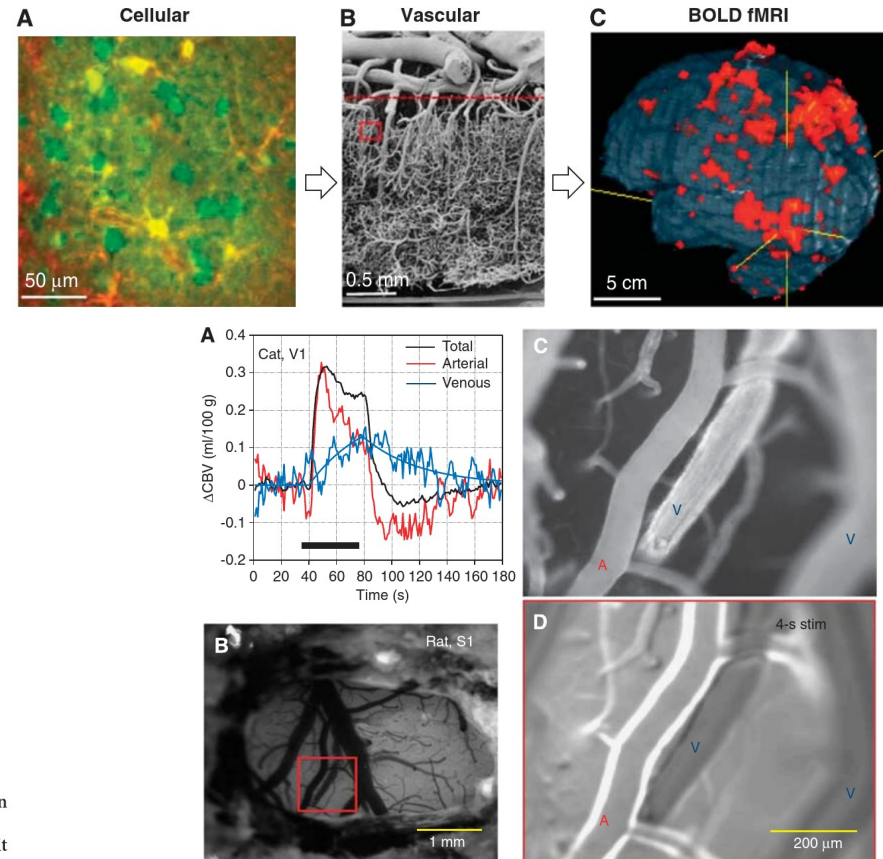
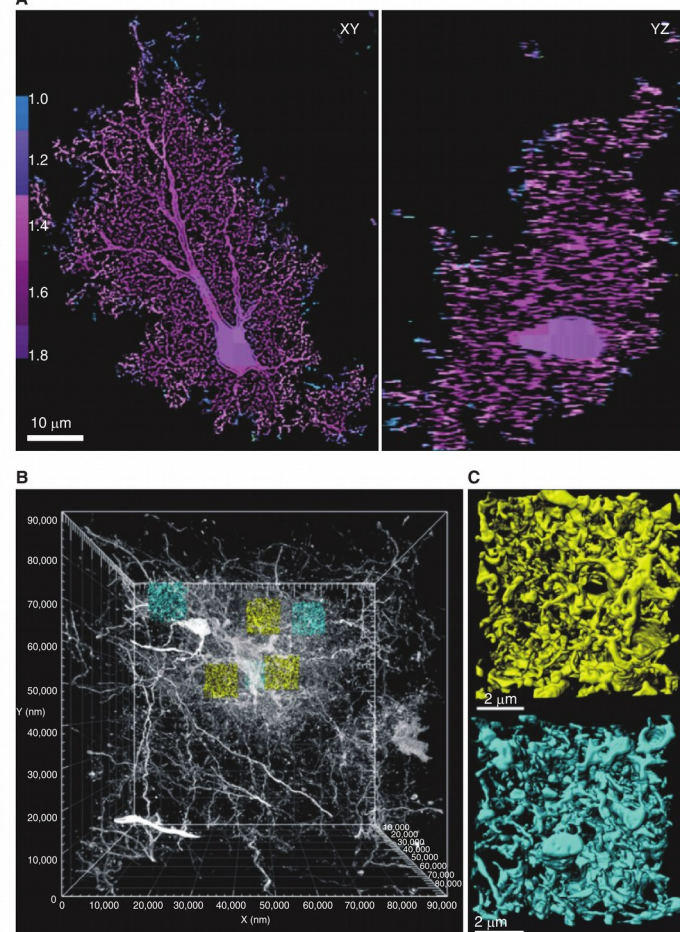
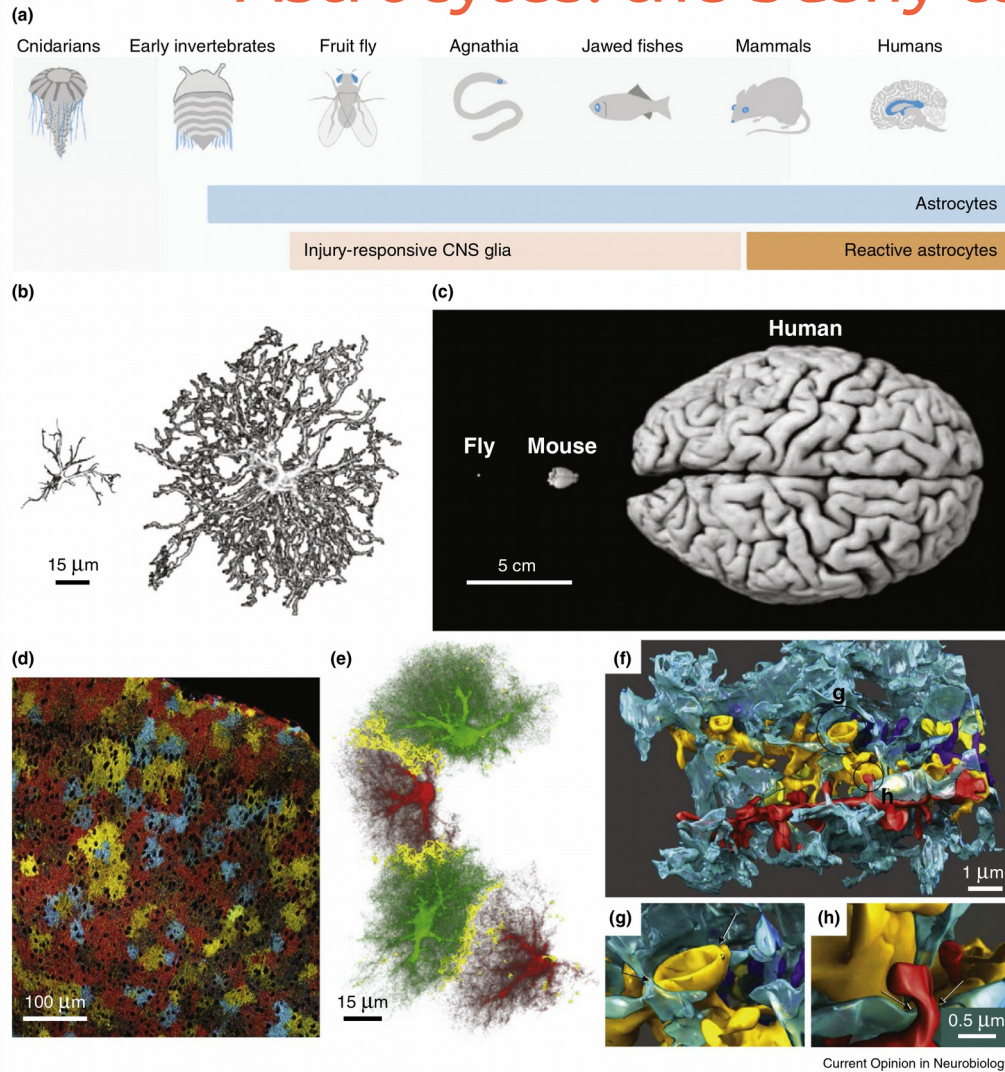


Figure 3 | Neural and vascular contents of a voxel. The left panel demonstrates the relative density of vessels in the visual cortex of monkeys. The dense vascular mesh is displayed by perfusing the tissue with barium sulphate and imaging it with synchrotron-based X-ray microtomography (courtesy B. Weber, MPI for Biological Cybernetics). The vessel diameter is colour coded. Cortical surface without pial vessels is displayed at the top; white matter at the bottom. At the left of the panel is a Nissl slice from the same area, showing the neural density for layers II through to the white matter (wm). Although the density of the vessels appears to be high in this three-dimensional representation, it is actually less the 3% (see section at the

right; white spots are cross-sections of vessels). The average distance between the small vessels (capillaries) is about 50 μm . This is approximately the distance that oxygen molecules travel by diffusion within the limited transit time of the blood. The dense population of neurons, synapses and glia occupy the intervascular space, as depicted in the drawing at the top right—a hypothetical distribution of vascular and neural elements in a small section (red rectangle). The drawing in the background shows some of the typical neuronal types (for example, red, large pyramidal cell; dark blue, inhibitory basket cells; light blue, chandelier inhibitory neurons; and grey, stellate cells) and their processes.



Astrocytes: the bushy cardinals of the CNS



Khakh, MacCarthy.
Cold Spring Harb Perspect Biol 2015;7:a020404

Astrocytes have Ca^{2+} excitability

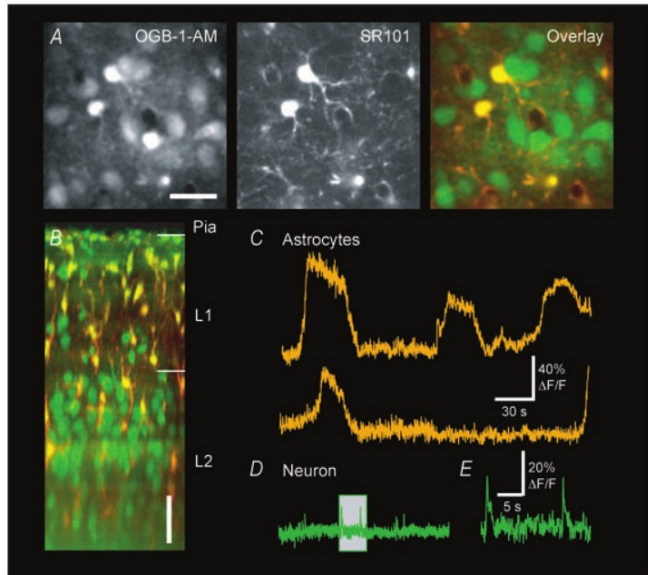


Figure 1. Calcium imaging of astrocytic and neuronal network excitation *in vivo*

A. Nimmerjahn, *J. Physiol.* (2009), **587**(8):1639-1647

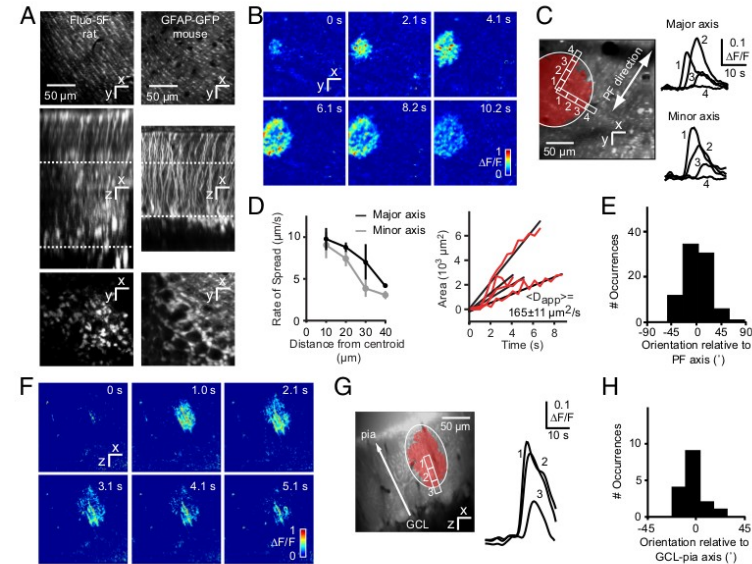


Fig. 1. Transglial calcium waves in the cerebellar cortex *in vivo*. (A) Staining patterns of the cerebellar cortex bolus-loaded with fluo-5F/AM (rat) or expressing GFP under the glial cell-specific GFAP promoter (mouse). (*Top*) Optical sections acquired in the molecular layer [ML, locations indicated by the upper dotted lines (*Middle*)] show a distinct striate pattern matching lateral protrusions from stem processes of Bergmann glia (BG). (*Middle*) Maximal side projection showing similarity between fluo-5F/AM labeling and GFAP-GFP expression. (*Bottom*) Optical sections taken from the Purkinje cell layer, with BG somata arranged around Purkinje cells. (B) Spontaneous radial wave measured in the ML. (C) Putative stem processes and side branches from BG show calcium increases with a time course typical of glial signals. (D) (*Left*) Wavefront slowing with distance from the initiation site. (*Right*) Linear rate of increase of wave area, with an average apparent diffusion constant $D_{app} = 165 \mu\text{m}^2/\text{s}$. Data are shown for 4 waves. (E) Distribution of wave orientation relative to the parallel fiber (PF) axis. (F) Radial wave in ML measured in an xz parasagittal plane orthogonal to the surface of the cerebellum. (G) Wave orientation along the axis of BG stem processes. (H) Distribution of wave orientation relative to the pia-Purkinje cell axis.

Hoogland et al, *PNAS* (2009), **106**(9) 3496-3501

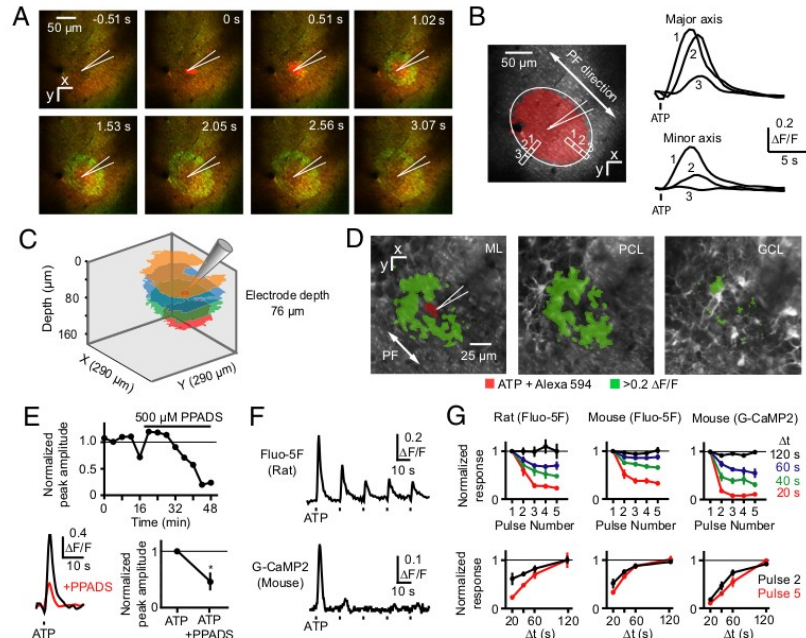
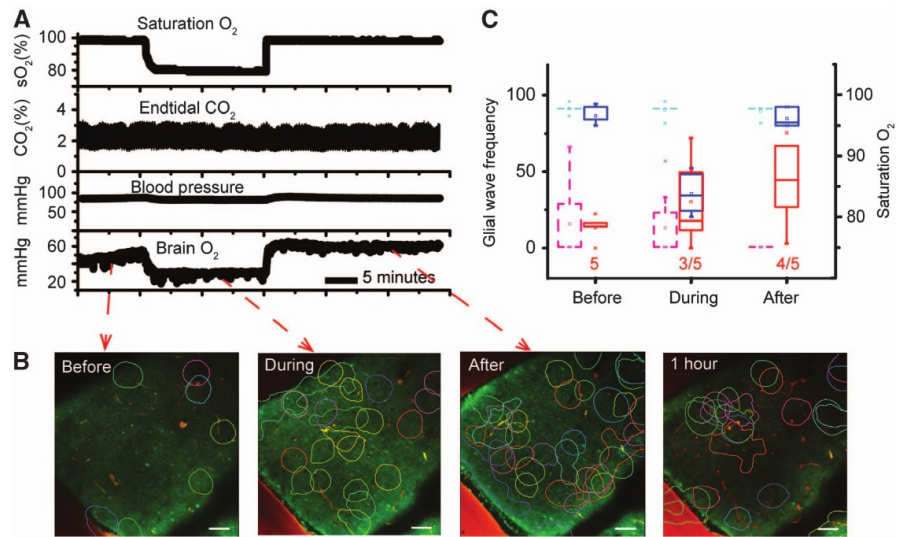
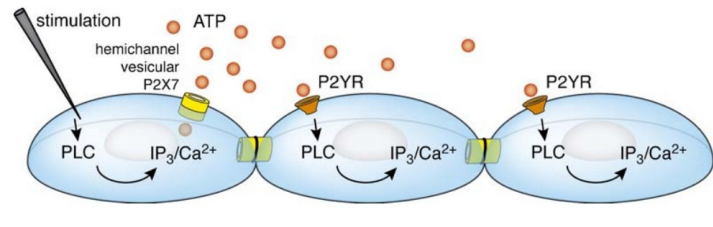


Fig. 4. ATP-triggered transglial calcium waves *in vivo*. (A) A transglial calcium wave evoked by ejection of ATP (pipette concentration: 1 mM, 10 ms, 0.07 bar) into the molecular layer. Green, Fluo-5F calcium signal; red, Alexa 594 and SR101. (B) Elliptical domain oriented along the PF axis in an ATP-triggered wave. (C) Waves triggered in rat cerebellar cortex at different imaging depths after ATP ejection at the same depth. (D) Activation of velate astrocytes in the granule cell layer after ATP ejection in lower third of the molecular layer, imaged by using G-CaMP2. (E) Reduction of ATP-triggered transglial signals by the P2 antagonist PPADS. (F) Decrease in successive calcium responses after repeated application of ATP. (G) Dependence of response amplitude after 5 pulses of ATP injected at different time intervals.

Hoogland et al, *PNAS* (2009), **106**(9) 3496-3501



Mathiesen, Brazhe, Thomsen, Lauritzen, *JCBFM* 2012

Optogenetics

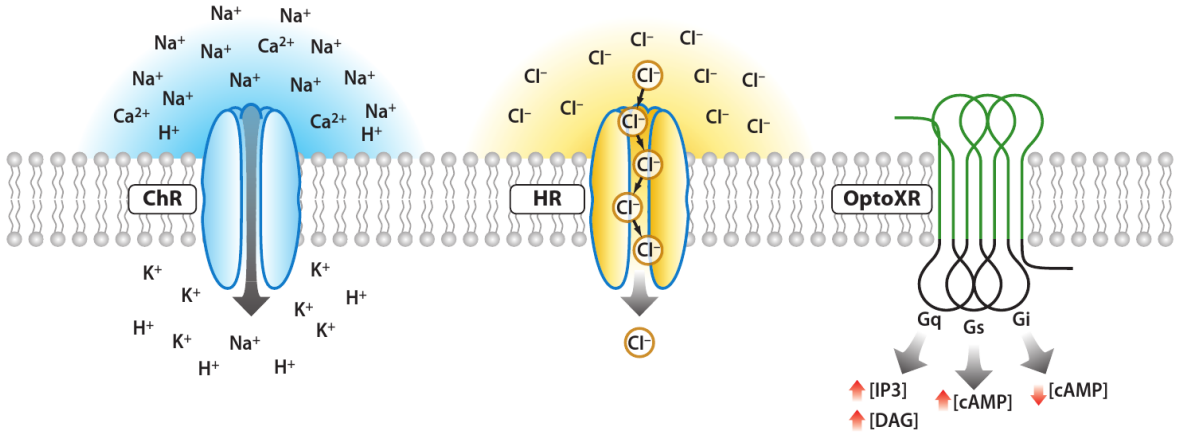


Figure 1

Optogenetic tool families. Channelrhodopsins conduct cations and depolarize neurons upon illumination (*left*). Halorhodopsins conduct chloride ions into the cytoplasm upon yellow light illumination (*center*). OptoXRs are rhodopsin-GPCR (G protein-coupled receptor) chimeras that respond to green (500 nm) light with activation of the biological functions dictated by the intracellular loops used in the hybrid (*right*).

Fenno et al 2011

